Title: Characterization of ADP-ribosyl cyclase 1-like (ARC1-like) activity and NAADP signaling during slow muscle cell development in zebrafish embryos

Running title: ARC1-like and NAADP in zebrafish slow muscle cell development

Jeffrey J. Kelu[1], Sarah E. Webb[1], Antony Galione[2] and Andrew L. Miller*[,1]

[1]Division of Life Science & State Key Laboratory of Molecular Neuroscience, HKUST, Hong Kong, [2]Department of Pharmacology, University of Oxford, Oxford, UK

*Correspondence: Andrew L. Miller, E-mail: almiller@ust.hk

Key Words: NAADP, ARC, Ca^{2+} signaling, Zebrafish, Slow muscle cells.

ABSTRACT

We recently demonstrated the requirement of two-pore channel type 2 (TPC2)-mediated Ca^{2+} release during slow muscle cell differentiation and motor circuit maturation in intact zebrafish embryos. However, the upstream trigger of TPC2/Ca^{2+} signaling during these developmental processes remains unclear. Nicotinic acid adenine dinucleotide phosphate (NAADP) is a potent Ca^{2+} mobilizing messenger, which is suggested to target TPC2 in mediating the release of Ca^{2+} from acidic vesicles. Here, we report the molecular cloning of the zebrafish ADP ribosyl cyclase (ARC) homolog (i.e., ARC1-like), which is the putative enzyme for generating NAADP. We characterized the expression of the *arc1-like* transcript and the NAADP level between ~16 hours post-fertilization (hpf) and ~48 hpf in whole zebrafish embryos. We showed that when ARC1-like was fused with either EGFP or tdTomato, it was localized in the plasma membrane, and associated with intracellular organelles, such as the acidic vesicles, Golgi complex and sarcoplasmic reticulum, in primary muscle cell cultures. Morpholino (MO)-mediated knockdown of *arc1-like* or pharmacological inhibition of ARC1 (via treatment with nicotinamide), led to an attenuation of Ca^{2+} signaling and disruption of slow muscle cell development. In addition, the injection of *arc1-like* mRNA into ARC1-like morphants partially rescued the Ca^{2+} signals and slow muscle cell development. Together, our data might suggest a link between ARC1-like, NAADP, TPC2 and Ca^{2+} signaling during zebrafish myogenesis.

HIGHTLIGHTS

- *Arc1-like* is expressed and NAADP detected from ~16 -48 hpf in zebrafish embryos.
- ARC1-like localize to the plasma membrane and organelles in slow muscle cells.
- ARC1-like expression and activity are required for slow muscle cell development.
- ARC1-like expression and activity are required for Ca^{2+} signaling in slow muscle cells.

INTRODUCTION

Ca^{2+} is a versatile second messenger that mediates a variety of cellular activities, including fertilization, differentiation, secretion, gene expression, muscle contraction, and apoptosis (Berridge, 2012). We previously showed that in zebrafish embryos two-pore channel (TPC) type 2 (TPC2)-mediated Ca^{2+} release is required for both slow muscle cell differentiation (Kelu et al., 2015; 2017), and early spinal circuit maturation (Kelu et al., 2018). TPCs are cation channels that conduct both Ca^{2+} and Na^{+} ions and their activity is mediated by multiple regulators (Jha et al., 2014; Galione, 2015), one of which is considered to be nicotinic acid adenine dinucleotide phosphate (NAADP). NAADP is a potent Ca^{2+} mobilizing messenger, which has been reported to activate TPC2 to release Ca^{2+} from the acidic vesicles (Calcraft et al., 2009; Ruas et al., 2015), perhaps by associating with an accessory NAADP-binding protein (Walseth et al., 2012; Lin-Moshier et al., 2012). However, details of when, where, and how NAADP is generated during vertebrate development remain unclear. To date, ADP-ribosyl cyclase (ARC) is the only known enzyme that has been demonstrated to synthesize NAADP (Lee, 2012; Fang et al., 2018). However, other enzymes have also been suggested to produce NAADP, utilizing methods other than the base-exchange reaction that occurs during ARC catalysis (Palade, 2007; Soares et al., 2007; Schmid et al., 2011).

ARC was first purified from the marine mollusk *Aplysia californica* (Lee and Aarhus, 1991). Studies suggest that it is a multi-functional enzyme that can utilize either nicotinamide adenine dinucleotide (NAD) or NAD-phosphate (NADP) as substrates to synthesize two structurally distinct Ca^{2+} mobilizing messengers (see reviews by Lee, 2011; 2012). These are cyclic adenosine diphosphate ribose (cADPR) and NAADP, which were shown to stimulate Ca^{2+} release from the endo-/sarco-plasmic reticulum (E/SR; Mészáros et al., 1993) and the acidic vesicles (Churchill et al., 2002), respectively. It was demonstrated that at neutral pH, ARC catalyzes the cyclization of NAD to generate cADPR; whereas at acidic pH, ARC catalyzes a base-exchange reaction, in which the nicotinamide group of NADP is replaced with nicotinic acid to generate NAADP (Lee, 2011; 2012). To date, ARC homologs have been identified in a wide range of animal species, including sea urchins (Churamani et al., 2007; Davis et al., 2008; Ramakrishnan et al., 2010), *Xenopus* (Churamani et al., 2012), mouse (Itoh et al., 1994), and humans (States et al., 1992), and overall they share ~20%-30% sequence identity (Ferrero et al., 2014).

CD38 was the first mammalian ARC homolog identified (States et al., 1992). Subsequent crystallography studies demonstrated that the structure of the C-terminal catalytic domain of CD38 is virtually identical to that of the *Aplysia* ARC (Prasad et al., 1996; Liu et al., 2005), even though the two proteins only share ~23% sequence identity. It was subsequently shown that in CD38-knockout mice, the stimulus-induced elevation of cellular NAADP, as well as the NAADP-mediated Ca^{2+} signaling, are

severely impaired (Cosker et al., 2010; Rah et al., 2010). These findings support the hypothesis that CD38 is required for the synthesis of NAADP *in vivo*. Based on sequence homology (Itoh et al., 1994) and structural resemblance (Yamamoto-Katayama et al., 2002), another mammalian homolog, CD157, (or BST-1) has been identified. However, the ability of CD157 to catalyze the synthesis of cADPR or NAADP remains unclear. For example, a recent study showed that CD157 was able to produce cADPR (at a far lower level than the CD38), but very little or no NAADP (Higashida et al., 2017).

Even though TPC2-mediated Ca^{2+} signaling was shown to play a key role during early zebrafish myotome development (Kelu et al., 2015; 2017), details regarding the signaling pathway(s) upstream of TPC2 are currently unclear. Here, we report the first molecular cloning of the zebrafish ARC homolog, i.e., ARC1-like, and the subsequent characterization of *arc1-like* expression and function during slow muscle cell development. Our data show that the *arc1-like* transcript is expressed between ~16 hours post-fertilization (hpf) and ~48 hpf, and the endogenous NAADP can also be detected in whole embryo extracts in the same developmental time window. This is the period when the zebrafish myotome (both slow and fast muscle cells) develop and are innervated by primary motor neurons (Jackson and Ingham, 2013; Plazas et al., 2013). We found that overexpressed ARC1-like fusion proteins were localized in the plasma membrane and in intracellular organelles in cultured primary muscle cells. Moreover, both the pharmacological inhibition of the ARC activity by nicotinamide and the molecular knockdown of the ARC1-like by a splice-blocking morpholino (MO-S; Morcos, 2007) led to severe disruption in myotomal patterning manifested by abnormal sarcomere formation, which indicates the importance of ARC1-like activity during slow muscle cell development. Importantly, NAADP production was reduced after nicotinamide treatment, supporting the requirement of ARC activity in generating NAADP *in vivo*. In addition, Ca^{2+} signaling in the slow muscle cells was attenuated after ARC1-like-knockdown, and this along with myotome patterning was partially rescued by the injection of *arc1-like* mRNA. Together, our new data might support the proposed action of an ARC1-like/NAADP/TPC2/Ca^{2+} signaling cascade in zebrafish during slow muscle cell development.

MATERIALS AND METHODS

Zebrafish husbandry and embryo collection

The AB wild-type zebrafish line and the smyhc1:GCaMP3 transgenic line (Jackson et al., 2015) were maintained, and their fertilized eggs collected, as previously described (Cheung et al., 2011). AB fish were obtained either from the Zebrafish International Resource Center (ZIRC; University of Oregon, USA), or the Biomedical Services Unit, John Radcliffe Hospital (University of Oxford, UK), whereas the smyhc1:GCaMP3 line was a gift from Prof. Philip Ingham (University of Exeter, UK). Fertilized eggs were maintained in Danieau's solution at ~28°C (Westerfield, 2000), or at room temperature (~23°C), to slow development until the desired stage was reached. All the procedures used in this study with live fish were performed in accordance with the guidelines and regulations set out by the Animal Ethics Committee of the HKUST and by the Department of Health, Hong Kong.

Identification of the ARC homolog in zebrafish

The National Center for Biotechnology Information (NCBI) HomoloGene database (https://www.ncbi.nlm.nih.gov/homologene) was used to search for and construct putative homology groups of the *ARC* gene from the complete gene sets of a wide range of eukaryotic species. As a result of this search, the *ADP-ribosyl cyclase/cyclic ADP-ribose hydrolase 1-like* gene (i.e., *arc1-like*; NCBI Gene ID: 101886891) was identified in zebrafish.

A subsequent multiple sequence alignment was performed using the NCBI Constraint-based Multiple Alignment Tool (COBALT; https://www.ncbi.nlm.nih.gov/tools/cobalt), and the results were then visualized using Jalview version 2.10.4b1 (Waterhouse et al., 2009). Residues that were in alignment were shaded using a graduated color scheme to highlight conservation using the "% identity" mode with a displaying threshold of 10.

Total RNA isolation, RT-PCR, and quantitative real-time PCR (qPCR)

Total RNA was extracted, cDNA was prepared, and RT-PCR was performed as previously described (Kelu et al., 2017) using whole embryos collected at ~16 hpf, ~18 hpf, ~20 hpf, ~22 hpf, ~24 hpf, and ~48 hpf. To detect the *arc1-like* transcript, the following primers were used: forward primer: 5'-TGGCAGGAGTTCGAAAAGGC-3', and reverse primer: 5'-GGATGGTTCAAACAGGCTGAC-3'. *β-actin* was used as an RT-PCR internal control (Kelu et al., 2017).

In addition, quantitative real-time PCR (qPCR) reactions were performed using 384-well plates (Roche Molecular Systems) on a LightCycler 480 Real-Time PCR System (Roche Molecular Systems), using ~50 ng RNA for each reaction. Primers were designed using the "Universal ProbeLibrary Assay Design Center" online tool (https://qpcr.probefinder.com/), and the following primers with their

corresponding universal probes (Roche Molecular Systems) were used: *arc1-like* forward primer: 5'-GGTTAATCCCAACCCCAAGT-3' (with probe #90); *arc1-like* reverse primer: 5'-ACAGCCTTTTCGAACTCCTG-3' (with probe #90); *actb2* forward primer: 5'-CCCTTGACTTTGAGCAGGAG-3' (with probe #38); *actb2* reverse primer: 5'-CAGGCAGCTCGTAGCTCTTC-3' (with probe #38); *ef1a* forward primer: 5'-AGCAGCAGCTGAGGAGTGAT-3' (with probe #77); *ef1a* reverse primer: 5'-CCGCATTTGTAGATCAGATGG-3' (with probe #77); *rpl13a* forward primer: 5'-TCCCGTGGATCATATCACTTC-3' (with probe #3); *rpl13a* reverse primer: 5'-GGTTTTGTGTGGAAGCATACC-3' (with probe #3). The qPCR cycling conditions comprised 95°C for 10 min, followed by 44 cycles of: 95°C for 10 sec; 60°C for 30 sec; and 72°C for 1 sec, and this was followed by 40°C for 30 sec. Samples were analysed with the LightCycler 480 system to attain Cp values. Standard curves were generated from serially-diluted pooled cDNA from all the samples analysed, and these were then used to determine the amplification efficiency (E), where $E \geq 95\%$ for all the genes analysed. The relative ΔCp for each gene was calculated by applying the formula $E^{(\text{lowest Cp-Cp})}$. Finally, the ΔCp for *arc1-like* was normalized to the geometric mean ΔCp of the three house-keeping genes (i.e., *actb2*, *ef1a*, and *rpl13a*; Vandesompele et al., 2002).

Construct preparation and *in vitro* transcription

Using cDNA that was prepared using oligo dT primers and total RNA extracted from whole embryos at ~24 hpf, the open reading frame (ORF) of *arc1-like* (i.e., 780 bp) was amplified via PCR using a high fidelity Platinum Taq DNA Polymerase (Invitrogen). The following primers were used: 5'-taatggtaccATGTTAGGTGCGAGAA-3' and 5'-cggcgaattcTCAAACATTAAAGTCAC-3', in which two restriction sites KpnI and EcoRI (denoted by the lowercase letters in the above sequences), were added to the 5' and 3' ends of the *arc1-like* ORF, respectively. The amplicons were then sub-cloned into the *pSP64TNE* plasmid (Cheung et al., 2006) to generate *pSP64TNE-zArc1-like*. To prepare *pSP64TNE-zArc1-like-EGFP* and *pSP64TNE-zArc1-like-tdTomato* constructs, the *arc1-like* ORF was amplified using the following primers: 5'-taatggtaccATGTTAGGTGCGAGAA-3' and 5'-taataccggtccAACATTAAAGTCACTGTCTGTGC-3', in which the stop codon was deleted and two restriction sites (i.e., KpnI and AgeI; lowercase letters), were added to the 5' and 3' ends, respectively. The amplicons were then sub-cloned into either the *pSP64TNE-EGFP* or *pSP64TNE-tdTomato* plasmid (Cheung et al., 2006), and this resulted in the in-frame fusion of the *arc1-like* ORF with the N-terminus of the EGFP or tdTomato fluorescent protein. The integrity of all the constructs generated was validated using Sanger sequencing analysis (Beijing Genomics Institute).

For *in vitro* transcription, the *pSP64TNE-zArc1-like*, *pSP64TNE-zArc1-like-EGFP*, and *pSP64TNE-zArc1-like-tdTomato* plasmids were first linearized using XbaI. The linearized templates were then

used to synthesize capped a*rc1-like*, *arc1-like-EGFP*, and *arc1-like-tdTomato* mRNAs using the mMESSAGE mMACHINE SP6 transcription kit (Ambion, Invitrogen Corp.). The mRNAs were then purified using phenol/chloroform extraction, diluted to ~100 to 200 ng/µL in DEPC-treated Milli Q, and stored at -80ºC.

NAADP extraction and cycling assay

Embryos at ~16 hpf, ~18 hpf, ~20 hpf, ~22 hpf, and ~24 hpf were dechorionated, immersed in 1.5 M perchloric acid and sonicated on ice to extract the NAADP. Endogenous nucleotides were removed and then the NAADP cycling assay was performed using well-established protocols (Graeff and Lee, 2013; Kelu et al., 2018).

Design and injection of MO oligomers and mRNAs, and evaluation of ARC1-like-knockdown efficacy

All the morpholino oligomers (MOs) used in this study were prepared by Gene Tools LLC. The standard control-MO, *p53*-MO, and *ARC1-like*-MO-S, were prepared and microinjected as previously described (Kelu et al., 2015; 2017; 2018). The *ARC1-like*-MO-S (i.e., 5'-ACCGAAATCATTGTGTTGTACCTCT-3') was co-injected with the *p53*-MO at ~1:1 ratio to alleviate potential off-targeting effects (Robu et al., 2007). Briefly, ~0.5 nL to ~2 nL of the diluted MOs were injected into the yolk of embryos at the 1- to 4-cell stage to reach a final amount of ~1 ng to ~5 ng. To evaluate the knockdown efficacy, RT-PCR was performed using the following primers: *ARC1-like*-MO-S-F: 5'-CCAGGCCATCCCTCAGATTT-3'; *ARC1-like*-MO-S-R: 5'-AGGTCCAGTGAAACCCTCGT-3'. Subsequently, 2% agarose gel electrophoresis was conducted to detect the presence of the aberrant transcript; whereas *β-actin* was used as an internal control. To rescue the morphant phenotype, ~1 nL (i.e., ~100 pg) of the capped a*rc1-like* mRNA was injected into the blastodisc of 1-cell stage embryos after the MO injection.

Overexpression of ARC1-like fusion proteins and fluorescent labelling of live primary cultured cells

To study the cellular localization of the ARC1-like fusion proteins, ~1 to 2 nL (i.e., ~100 to 200 pg) of either the *arc1-like-EGFP* or *arc1-like-tdTomato* mRNA was injected into the blastodisc of wild-type embryos at the 1-cell stage. Whole embryos were dissociated at ~48 hpf and primary cell cultures were prepared following procedures described previously (Kelu et al., 2017). The dissociated cells were cultured on laminin-coated coverslips (18-mm diameter; No. 1; Paul Marienfeld GmbH & Co. KG) for 1 h at room temperature, after which they were labelled using: 5 µg/mL FM 4-64 (#T3166), 500 nM LysoTracker Red DND-99 (#L7528), 2 µM ER-Tracker Green (#E34251), or 5 µM BODIPY FL C5-ceramide (#D3521). All of these florescent dyes were purchased from Invitrogen, and the stock

solutions were prepared in DMSO and then stored at -20°C. Just prior to use, most of the dyes were prepared in sterile Live Cell Imaging Solution (140 mM NaCl; 2.5 mM KCl; 1.8 mM $CaCl_2$; 1 mM $MgCl_2$; 20 mM HEPES; pH 7.4; recipe provided by Invitrogen), containing 5 mM filtered D-glucose. However, as FM 4-64 requires Mg^{2+}/Ca^{2+}-free conditions, it was prepared in sterile phosphate-buffered saline (PBS) at pH 7.3. Most of the dye labelling procedures were conducted at room temperature for 30 min. However, the FM 4-64 and BODIPY FL C5-ceramide labelling protocols were conducted on ice for 1 min and 30 min, respectively.

With most of the dyes, the cells were washed thoroughly with the Live Imaging Solution after labeling and prior to imaging. However, the FM 4-64-labelled cells were kept in the staining solution for imaging, which was completed within 15 min. To image the fluorescently labelled cells, laser scanning confocal microscopy was conducted using a Leica TCS SP5 II confocal system and images were acquired using a Leica HCX PL APO 40X/1.25-0.75 NA oil immersion objective lens. Green fluorescence was captured using 488 nm excitation and 519 nm detection; whereas red fluorescence was captured with 543 nm excitation and 570 nm detection. Images from the green and red channels were sequentially obtained. The temperature was maintained at ~28°C throughout imaging.

Whole-mount immunohistochemistry and fluorescent labelling of fixed embryos

Embryos fixed at ~24 hpf were labelled with the anti-myosin heavy chain (F59) primary antibody (used at 1:5; Developmental Studies Hybridoma Bank). The subsequent secondary antibody incubation was conducted with an Alexa Fluor 488 or 546 goat anti-rabbit IgG (H+L) antibody (used at 1:200; Molecular Probes), after which embryos were then co-labelled with Alexa Fluor 568 or 488-tagged phalloidin (used at 1:50; Molecular Probes), respectively. Embryos were fixed and immunolabelled following procedures described previously (Kelu et al., 2015; 2017). Prior to mounting, the yolk and the head of the labelled embryos were both excised and discarded, and then the trunk was mounted on microscope slides using Aqua-Poly/Mount (Polysciences, Inc.).

To image the fluorescently-labelled embryos, laser scanning confocal microscopy was conducted using either a Leica TCS SP5 II or a Zeiss LSM 510 META confocal system. For the Leica confocal system, images were acquired using a Leica HCX PL APO 63X/1.4-0.6 NA oil immersion objective lens; and green fluorescence was captured using 488 nm excitation and 519 nm detection; whereas red fluorescence was captured with 543 nm excitation and 570 nm detection. For the Zeiss confocal system, images were acquired using a Zeiss Plan-Apo 63X/ NA 1.4 oil immersion objective lens; and green was captured using 488 nm excitation and 505-530 nm emission; whereas red fluorescence was captured with 543 nm excitation and >560 nm emission. Images from the green and red channels were sequentially obtained, and the confocal z-stacks of images acquired were

reconstructed using Fiji (NIH). Various parameters of the myotome of embryos were measured using Fiji, as previously described (Kelu et al., 2017).

Confocal imaging of live smyhc1:GCaMP3 transgenic embryos

To image Ca^{2+} transients generated in the slow muscle cells, dechorionated smyhc1:GCaMP3 transgenic embryos (controls, MO- and MO + mRNA-injected) at ~18 hpf or ~24 hpf were embedded in 2% low gelling temperature agarose and then orientated lateral side down in a glass-bottomed cultured dish (MatTek) to restrict their motility. Series of time-lapse fluorescence images were then obtained from a lateral view in the region of the trunk where the slow muscle cells are located, at ~8.93 Hz for a period of ~180 s. GCaMP3 fluorescence was acquired with the Leica TCS SP5 II confocal system, using 488 nm excitation and 519 nm detection via a Leica HC PL APO 20X/ 0.7 NA objective lens with the pinhole fully open at 600 µm. The power of the laser and other imaging parameters were kept constant for all the experiments, and the temperature was maintained at ~28°C throughout imaging. To detect GCaMP3 fluorescence generated in the slow muscle cells in the smyhc1:GCaMP3 transgenic embryos, rectangular regions of interest (ROIs; each with an area of ~200 μm^2), were positioned on the center of five slow muscle cells using Fiji. The frequencies and amplitudes of GCaMP3 fluorescence were quantified as previously described (Kelu et al., 2018).

Pharmacological treatments

Stock solutions of 500 mM nicotinamide and benzamide (Sigma-Aldrich Corp.) were prepared in Danieau's solution and stored at -80°C. Dilutions were done using Danieau's solution just prior to use: Nicotinamide was diluted to 1 mM, 10 mM, or 50 mM; whereas benzamide was diluted to 50 mM. Nicotinamide or benzamide was applied to embryos at ~17 hpf after tail-cut as described previously (Kelu et al., 2015; 2017; 2018), and the temperature was maintained at ~28°C for the duration of each experiment. A control group was also prepared by incubating tail-cut embryos in Danieau's solution alone.

Statistical analysis

Numerical data were exported to Minitab 18.1.0 for statistical analysis. The following non-parametric tests were then conducted: the Mann-Whitney Test (for comparison between two groups), and the Kruskal-Wallis Test (for comparison between multiple groups). The latter test was followed by the post-hoc Dunn's Test to determine statistical significance in individual comparison pairs. $P < 0.05$ was considered to be statistically significant.

RESULTS

Identification of the zebrafish ARC homolog

Putative ARC homologs were identified with the NCBI HomoloGene Database. The results suggest that the *arc* gene is conserved in the clade Euteleostomi (which includes >90% of the living species of vertebrates). In our homology search, one zebrafish *arc* gene, (i.e., *ADP-ribosyl cyclase/cyclic ADP-ribose hydrolase 1-like*), was identified along with the well-studied mammalian *arcs* (i.e., *cd38* and *bst-1*; States et al., 1992; Itoh et al., 1994), and sea urchin (*Strongylocentrotus purpuratus*) *arcs* (i.e., *arc1-arc4;* Churamani et al., 2007; Davis et al., 2008; Ramakrishnan et al., 2010). We successfully cloned the zebrafish *arc* homolog from cDNA prepared at ~24 hpf, and then sub-cloned it into the *pSP64TNE* plasmid (Cheung et al., 2006) for Sanger sequencing analysis. The sequencing results confirmed that the putative open reading frame of the zebrafish *arc* homolog is 780 bp long, which corresponds to a 259 amino acid peptide with a molecular weight of ~30 kDa. Multiple sequence alignments of the zebrafish ARC homolog with other members of the ARC family revealed modest sequence identity and similarity at the amino acid level (Table 1). Our results showed that the zebrafish (*Danio rerio*) *Dr*ARC shares 34% identity and 55% similarity with human ARC1 (*Hs*CD38); 37% identity and 53% similarity with human ARC2 (*Hs*BST1); 34% identity and 55% similarity with mouse ARC1 (*Mm*CD38); and 36% identity and 51% similarity with mouse ARC2 (*Mm*BST1; Table 1). *Dr*ARC also shares a significant but lower sequence identity and similarity with the sea urchin ARCs (*Sp*ARC1-4), with sequence identities ranging from 26% to 30%, and sequence similarities ranging from 42% to 48% (see Table 1). Due to the sequence similarity of the zebrafish *arc*/ARC homolog to the mammalian *arc1s*/ARC1s, it is thus referred to as *arc1-like*/ARC1-like. The accession number of the protein sequences of the ARC homologs are as follows: BAA18966.1 (human CD38), AAH12095.1 (human BST1), CAJ18593.1 (mouse CD38), BAA06597.1 (mouse BST1), XP_021325948.1 (zebrafish ARC1-like), CAM36041.2 (sea urchin ARC1), CAM36042.3 (sea urchin ARC2), CAM36043.1 (sea urchin ARC3), and NP_001243005.1 (sea urchin ARC4).

Further investigations were conducted to study the putative protein architecture of the various ARC homologs, and a common conserved domain was identified. Our results from an NCBI Conserved Domain Search suggested that all the ARC homologs possess a conserved “Rib_hydrolase” domain (accession number: pfam02267; Fig. S1), which constitutes a characteristic substrate-binding site (Liu et al., 2006; Fig. S1). Despite the limited amino acid sequence homology (Table 1), there is absolute conservation of the ten residues that compose this conserved feature, the positions of which were mapped to the domain architecture of the ARC homologs (see red lines in Fig. S1). A multiple protein sequence alignment diagram was constructed to provide a higher resolution study of the level of conservation among the various ARC homologs (Fig. 1). Our results indicate the presence of strong

conservation at multiple positions in the alignment as revealed by the graduated color scheme (i.e., residues shaded in blue) and the histogram (i.e., columns with a score of "*"; Fig. 1). These include cysteine residues (see the residues shown in yellow in Fig. 1), which are involved in disulphide bond formation (Prasad et al., 1996; Liu et al., 2005). It should be noted that eight cysteine residues were found in *Dr*ARC1-like (see Fig. 1). In addition, ten residues that are known to be important for substrate binding (Liu et al., 2006) are well-conserved in *Dr*ARC1-like (see red lines in Fig. S1 and the residues shown in red in Fig. 1). Moreover, there is a high level of conservation in the glutamic acid residue at position 268 of the alignment (see Fig. 1); this is equivalent to Glu-226 in human CD38, which was shown to be important for the catalytic activity of this ARC (Munshi et al., 1999).

Detection of the *arc1-like* transcript and endogenous NAADP in zebrafish embryos during late segmentation

To investigate the expression pattern of *arc1-like*, total RNA was extracted from whole embryos at ~16 hpf, ~18 hpf, ~20 hpf, ~22 hpf, ~24 hpf, and ~48 hpf. Using RT-PCR, *arc1-like* was shown to be expressed at a low level between ~16 hpf and ~20 hpf (Fig. 2A). The expression of *arc1-like* started to increase at ~22 hpf, and it reached the highest level (of all the time points tested) at ~48 hpf (Fig. 2A). To quantify the fold-change in *arc1-like* expression, qPCR was performed (Fig. 2B), and *arc1-like* was normalized to three house-keeping genes (i.e., *actb2*, *ef1a*, and *rpl13a*). The qPCR data recapitulated the RT-PCR results, such that *arc1-like* was detected at a low level between ~16 hpf and ~20 hpf, and it exhibited a significant increase at ~22 hpf (at $p<0.05$), ~24 hpf (at $p<0.01$), and ~48 hpf (at $p<0.01$; i.e., by ~4-fold, ~6-fold, and >100-fold, respectively), when compared with the level at ~16 hpf (Fig. 2B).

The NAADP cycling assay was conducted to measure the endogenous level of NAADP in whole embryos at the same stages of development used for the RT-PCR and qPCR (Fig. 2C). In this fluorometric assay, the increase in resorufin fluorescence over time reflects the [NAADP] in the samples under investigation. A series of NAADP standards was assayed along with the zebrafish NAADP extracts (Fig. S2A). As determined from the NAADP standard curve, the rate of resorufin fluorescence change increased linearly with the increase in NAADP concentration (with an $R^2>0.99$); this validated the efficacy and reliability of the cycling assay (Fig. S2B).

To control for the difference in cell number of embryos at different developmental stages, the [NAADP] detected was initially normalized to the protein amount of the corresponding extracts (Fig. S2C), before being compared with that at ~16 hpf (Fig. 2C). The results showed that there was no significant difference in the [NAADP] in embryos at ~18 hpf, ~22 hpf, and ~48 hpf (Fig. 2C). However, the [NAADP] decreased significantly at ~20 hpf (i.e., exhibiting ~40% decrease when compared with

the ~16 hpf level; at $p<0.05$), and then at ~24 hpf, the [NAADP] decreased further (i.e., by ~60% when compared with the ~16 hpf level; $p<0.001$). By ~48 hpf, the [NAADP] had returned back to a somewhat similar level as that observed at ~16 hpf (Fig. 2C).

Characterization of the cellular localization of ARC1-like fusion proteins

To examine the cellular localization of the ARC1-like, ARC1-like-EGFP or ARC1-like-tdTomato was transiently overexpressed in wild-type embryos via the injection of the capped *arc1-like-EGFP* (Fig. 3Ai, 3Bi) or *arc1-like-tdTomato* (Fig. 3Ci, 3Di) mRNAs respectively, at the 1-cell stage. Primary cultures were then prepared from the injected embryos at ~48 hpf, and the cells were labelled with different cell-permeant fluorescent dyes, i.e., FM 4-64 (Fig. 3Aii), LysoTracker Red DND-99 (Fig. 3Bii), BODIPY FL C5-ceramide (Fig. 3Cii), or ER-Tracker Green (Fig. 3Dii), to visualize the plasma membrane, acidic vesicles, Golgi complex, or sarcoplasmic reticulum (SR), respectively. Live imaging was performed on the muscle cells, which were identified based on the elongated appearance and/or the presence of striations when visualized by confocal microscopy.

The confocal imaging data showed that ARC1-like-EGFP was localized in the plasma membrane (see white arrowhead in Fig. 3A*), and in the acidic vesicles (see white arrowhead in 3B*). In the single optical section showing ARC1-like-EGFP and acidic vesicles, both were distributed in a striated pattern in the cytoplasm and what we suggest is a peri-nuclear location in the cell (Fig. 3Bi, 3Bii). ARC1-like-tdTomato clusters were localized with the Golgi complex (see white arrowhead in Fig. 3C*), and the SR (see white arrowheads in Fig. 3D*).

Effect of nicotinamide on the development of the slow muscle cells

To investigate the possible function of ARC in the development of the zebrafish myotome, embryos that had the end of the tail excised, were treated with either Danieau's solution alone (Fig. 4A, 4A*) or Danieau's solution containing nicotinamide at 1 mM (Fig. 4Bi, 4Bi*), 10 mM (Fig. 4Bii, 4Bii*), or 50 mM (Fig. 4Biii, 4Biii*). Embryos were treated from ~17 hpf to ~24 hpf and then they were fixed and labelled to visualize F-actin and the myosin heavy chain (Fig. 4A, 4B). Our results showed that nicotinamide impeded the development of the slow muscle cells in a dose-dependent manner. At 1 mM, the organization of the myofibrils was maintained, but the width of the myotome was decreased (Fig. 4Bi). In addition, the sarcomeres remained relatively normal (compare Fig. 4Bi* with Fig. 4A*). At 10 mM, the slow myofibers exhibited a slightly more disorganized and flexuous morphology, and the width of myotome was further decreased (Fig. 4Bii), but the normal sarcomeric banding pattern was still apparent (compare Fig. 4Bii* with Fig. 4A*). At 50 mM, however, the myotome and individual myofibers exhibited an obvious decrease in width, and the slow myofibers were more obviously

disorganized and flexuous (Fig. 4Biii). Moreover, the sarcomeric patterning in the myofibrils was lost (Fig. 4Biii*).

To quantify the effect of the 50 mM nicotinamide treatment, the same set of criteria used in the Kelu et al. (2017) study was used to measure the myotome width (Fig. 4C), the somite angle (Fig. 4D), the amount of straightness of the myofibers (Fig. 4E), and the myofiber width (Fig. 4F). To determine the extent of myofiber straightness, the myofiber:somite length ratio was calculated, where a value >1 indicates the presence of more flexuous slow myofibers (Kelu et al., 2017). The results of the statistical analysis revealed that all the parameters (except the somite angle) were significantly different from the control at $p<0.001$ (Fig. 4C-4F). Taken together, these data suggest the requirement of ARC activity during the normal development of the zebrafish myotome. To evaluate the inhibitory effect of 50 mM nicotinamide further, the endogenous level of NAADP was measured in both untreated control and 50 mM nicotinamide-treated embryos at ~24 hpf using the NAADP cycling assay (Fig. 4Gi). The results show that in the nicotinamide-treated embryos, the production of NAADP was significantly reduced (at $p<0.05$), when compared with that in the untreated control embryos (Fig. 4Gi). To illustrate the selectivity of nicotinamide for ARC inhibition, in some experiments embryos were treated with 50 mM benzamide, a chemical compound that is structurally similar to nicotinamide, except that the nitrogen atom (N) in the pyridine ring of nicotinamide is replaced by a methine group (=CH-), which forms a benzene ring (Fig. 4Gii). The results show that in the benzamide-treated embryos, the production of NAADP was not significantly different from the untreated controls (Fig.4Gi).

Effect of MO-based knockdown of ARC1-like on the development of the slow muscle cells

To study the function of the *arc1-like* gene in further detail, an *ARC1-like*-MO-S was designed to interfere with the normal splicing of the *arc1-like* pre-mRNA at the exon 5-intron 5 junction (Fig. S3A). A dose-response chart was constructed to determine the optimal *ARC1-like*-MO-S dose (Stainier et al., 2017; Fig. S3Bi). To circumvent potential off-targeting effects, the *ARC1-like*-MO-S was co-injected with *p53*-MO at a 1:1 ratio (Kelu et al., 2015; 2017; 2018). Thus, embryos were injected at the 1- to 4-cell stage with: ~5 ng of standard control-MO; ~5 ng *p53*-MO; ~1 ng *ARC1-like*-MO-S + ~1 ng *p53*-MO, ~2 ng *ARC1-like*-MO-S + ~2 ng *p53*-MO, or ~5 ng *ARC1-like*-MO-S + ~5 ng *p53*-MO (Fig. S3Bi). In contrast to the control embryos, the ARC1-like morphants were observed to display failure in the straightening of the trunk at ~24 hpf, ranging from mild to severe (Fig. S3Bii). The efficacy of MO knockdown was evaluated using RT-PCR with a pair of primers that flanks the targeted locus of *arc1-like* (Fig. S3A, S3C). An aberrant (lower molecular weight) transcript was detected in the morphants (but not in the controls) after gel electrophoresis (Fig. S3C). We suggest that this might be due to exon

5 (which consists of 139 bases; i.e., non-divisible by 3) being skipped (Fig. S3A, S3C; Morcos, 2007). If this is the case, then it might result in a frameshift in the downstream sequence, which would subsequently lead to a loss of most, if not all of the conserved residues that are downstream of lys-98 (see Fig. 1).

To examine the status of muscle development following ARC1-like-knockdown, F-actin and myosin heavy chain, were again visualized using fluorescently-labeled phalloidin and via immunolabelling with the F59 antibody, respectively. Labelling was performed on whole-mount embryos (at ~24 hpf) that were injected at the 1- to 4-cell stage with: ~5 ng standard control-MO (Fig. 5A); ~5 ng *p53*-MO (Fig. 5B); ~1 ng *ARC1-like*-MO-S + ~1 ng *p53*-MO (Fig. 5Ci); ~2 ng *ARC1-like*-MO-S + ~2 ng *p53*-MO (Fig. 5Cii); or ~2 ng *ARC1-like*-MO-S + ~2 ng *p53*-MO + ~100 pg *arc1-like* mRNA (Fig. 5D). When the F-actin and myosin heavy chain images were superimposed, the morphology of the myotome and somites as well as the width and shape of the myofibers were revealed at low magnification (Fig. 5A-5D), whereas information regarding the sarcomeric structure was revealed at high magnification (Fig. 5A*-5D*). While the development of the trunk musculature was observed to be normal in the control embryos (Fig. 5A, 5B), the myotome and myofiber widths were reduced, and the myofibers were less organized in the morphants injected with ~1 ng *ARC1-like*-MO-S (see white arrows in Fig. 5Ci). A more severe phenotype was exhibited by the morphants injected with ~2 ng *ARC1-like*-MO-S, such that the myofibers exhibited more disorganized flexuous phenotype (see white arrows in Fig. 5Cii). After co-injection of *ARC1-like*-MO-S and *arc1-like* mRNA, however, the morphology of the myofibers (and hence the myotome) was rescued to a large extent (Fig. 5D). The high magnification images (Fig. 5A*-5D*) showed that the usual striated pattern of the sarcomeres observed in the control embryos (Fig. 5A*, 5B*) was absent in the morphants (Fig. 5Ci*, 5Cii*). In addition, fractures in the myofibers could be observed in the morphants at higher magnification (see white arrowheads in Fig. 5Cii*). Again, the co-injection of *arc1-like* mRNA with the *ARC1-like*-MO-S somewhat restored the normal banding pattern in the slow myofibrils (Fig. 5D*).

Measurements were made to quantify the changes in muscle morphology after ARC1-like-knockdown (Fig. 5E-5H). The data show that the myotome width and myofiber width were significantly decreased, whereas the myofiber length:somite length were significantly increased (all at $p<0.001$) in the morphants injected with ~2 ng *ARC1-like*-MO-S when compared with the controls (Fig. 5E, 5G, 5H). In addition, the myotome width and myofiber width were significantly increased and the myofiber length:somite length were significantly decreased (all at $p<0.001$) in the morphants coinjected with *arc1-like* mRNA (Fig. 5E, 5G, 5H). This suggests that the *ARC1-like*-MO-S-induced defects could be at least partially rescued. The *ARC1-like*-MO-S appeared to have no effect on the shape of the somites

such that the somite angle (defined in Kelu et al., 2017), was not significantly affected in the morphants, when compared with the controls (Fig. 5F).

Effect of MO-based knockdown of ARC1-like on the Ca^{2+} signaling of the slow muscle cells

The function of ARC1-like on regulating the Ca^{2+} signaling in the developing myotome was investigated using the smyhc1:GCaMP3 transgenic line, which expresses a genetically-encoded Ca^{2+} indicator, GCaMP3, specifically in the slow muscle cells (Jackson et al., 2015; Fig. 6). Transgenic embryos that were untreated, or else injected with: standard control-MO; *p53*-MO; *ARC1-like*-MO-S + *p53*-MO; or *ARC1-like*-MO-S + *p53*-MO + *arc1-like* mRNA, were imaged in a lateral orientation at ~18 hpf (Fig. 6A) and ~24 hpf (Fig. 6B) over a period of ~180 s to visualize the Ca^{2+} dynamics in individual slow muscle cells. To quantify the frequency and amplitude of the Ca^{2+} transients, regions of interest (ROIs) were placed over selected slow muscle cells (n=15 to 30, from 3 to 6 embryos; Fig. 6Ai, 6Bi), and Ca^{2+} signaling profiles from the representative ROIs were generated (Fig. 6Aii, 6Bii). At ~18 hpf, distinct Ca^{2+} signals were observed in the various control groups (i.e., the untreated, and the standard control-MO- or *p53*-MO-injected groups). In contrast, the Ca^{2+} signaling activity was highly attenuated in the morphants, whereas there was an increase in the frequency and amplitude of the Ca^{2+} signaling activity in the rescue group when compared with the morphants (Fig. 6Aii). A similar pattern of Ca^{2+} signaling activity was observed at 24 hpf, such that the activity was attenuated in the morphants when compared with the controls (Fig. 6Bii), whereas the Ca^{2+} signals appeared to be restored when *ARC1-like*-MO-S was co-injected with *arc1-like* mRNA (Fig. 6Bii). Quantification and statistical analysis suggested that at both ~18 hpf and ~24 hpf, the frequency (Fig. 6Aiii, 6Biii) and amplitude (Fig. 6Aiv, 6Biv) of the Ca^{2+} signals in the morphants were significantly lower (at $p<0.001$) than those in the controls, whereas the frequency and amplitude of the Ca^{2+} signals in the rescued embryos were significantly higher (at $p<0.01$ or $p<0.001$) than those in the morphants. These data also show that in all of the control groups, the frequency and amplitude of the Ca^{2+} signals were significantly higher at ~18 hpf than at ~24 hpf (Fig. 6Ci, 6Cii). However, in the *ARC1-like*-MO-S alone, and *ARC1-like*-MO-S + *arc1-like* mRNA groups, no significant differences were observed when comparing the frequency or amplitude at these two time points.

Importantly, the inhibitory effect of *ARC1-like*-MO-S on the generation of Ca^{2+} signals was phenocopied by treatment of smyhc1:GCaMP3 embryos with 50 mM nicotinamide (via tail-cut) at ~17 hpf for 1 h (Fig. S4A). At ~18 hpf, both the frequency and amplitude of the slow muscle cell-generated Ca^{2+} signals decreased significantly (at $p<0.001$ and $p<0.01$, respectively) after nicotinamide treatment when compared with the untreated controls (n=15 to 25, from 3 to 5 embryos; Fig. S4B, S4C).

DISCUSSION

We have recently reported the importance of TPC2-mediated Ca^{2+} signaling during slow muscle cell development (Kelu et al., 2015; 2017) and myotome innervation by primary motor neurons (Kelu et al., 2018). Thus, the investigation of NAADP synthesis and regulation might help identify a key component of the upstream mechanistic pathway as to how TPC2/Ca^{2+} signaling might contribute to the regulation of these developmental processes. To date, ARC remains the only known enzyme that has been reported to synthesize NAADP (Lee, 2012; Fang et al., 2018); however, the molecular characterization of ARC has only been conducted in a few organisms (Ferrero et al., 2014). Here, we report the application of a bioinformatics approach (by sequence comparison), to identify a putative ARC homolog, called ARC1-like, in zebrafish. Although the zebrafish ARC1-like only shows modest amino-acid sequence identity with the other ARC homologs (i.e., ~26-37%; see Table 1), there is an excellent conservation of the cysteine residues (involved in disulphide bond formation), which are required for the enzymatic activity of ARC (Prasad et al., 1996; Liu et al., 2005), as well as other residues suggested to be important for substrate binding (Liu et al., 2006), and catalysis (Munshi et al., 1999; Figs 1, S1). These conserved residues might, therefore, result in functional similarities between the homologues, i.e., the synthesis of NAADP (Figs 2C, S2). Thus, we attempted to clone *arc1-like* and then characterize ARC1-like by: 1) Studying the expression levels of the *arc1-like* transcript (Fig. 2A, 2B); 2) Detecting the endogenous levels of NAADP in whole embryos (Figs 2C, S2); and 3) Studying the localization of ARC1-like fusion proteins in primary cultured muscle cells (Fig. 3).

We showed that the *arc1-like* transcript was expressed throughout the period of neuromuscular development in zebrafish (Jackson and Ingham, 2013; Plazas et al., 2013), with a gradual increase in expression from ~16 hpf to ~24 hpf, followed by a substantial increase between ~24 hpf and ~48 hpf (Fig. 2B). In contrast, a significant reduction in the level of endogenous NAADP was detected in whole embryos between ~16 hpf and ~24 hpf, with a subsequent rise between 24 hpf and 48 hpf (Fig. 2C). The reason for the mis-match between the levels of the *arc1-like* transcript and NAADP might be due to a number of factors (compare Fig. 2C with 2A and 2B). For example, accumulating evidence regarding the regulation of NAADP production suggests that the mammalian ARC homolog CD38 is constitutively active, and therefore the regulation of its activity is dependent on the availability of substrate (Howard et al., 1993; Deshpande et al., 2005; Lee, 2012). Indeed, it was recently suggested that the synthesis of NAADP by CD38 might be limited by the availability of nicotinic acid (which is the substrate for the base-exchange reaction by ARCs), and that the yield of NAADP can be greatly enhanced by supplementing cells with nicotinic acid (Fang et al., 2018). Thus, the high level of expression of *arc1-like* does not necessarily result in a high level of ARC activity (i.e., NAADP production), but rather that ARC activity is limited by the availability of substrate. It has also been

suggested that ARC is responsible for hydrolyzing NAADP *in vivo* (Schmid et al., 2011; Guse and Diercks, 2018). Therefore, in zebrafish embryos, NAADP might accumulate and remain at a high level at 16 hpf and 18 hpf when its degradation rate is hindered by the low abundance of ARC at these stages. In contrast, when the expression of ARC becomes higher at the later stages, then the level of NAADP might decrease as more is degraded (Fig. 2). Although the nature of ARC function as well as its regulation during development remains to be investigated in further detail, the presence of both *arc1-like* transcripts and endogenous NAADP support previous reports that indicate essential TPC2/Ca^{2+} activity occurs in zebrafish between ~16 hpf and ~48 hpf (Kelu et al., 2015; 2017; 2018).

To study the localization of the zebrafish ARC1-like, we utilized a primary muscle cell culture system (Kelu et al., 2017; Fig. 3). Our results showed that ARC1-like-EGFP was expressed in the plasma membrane (Figs. 3Ai, 3Aii and 3A*); they therefore support previous findings from human lymphocytes, where CD38 was identified as being a cell surface transmembrane protein (Jackson and Bell, 1990). Such an ectocellular (i.e., cell surface) localization of ARCs is also supported by recent observations that overexpressed CD38-Myc localizes in the plasma membrane in *Xenopus* embryos (Churamani et al., 2012). In addition, in human HL-60 cells, endogenous CD38 was shown to be expressed at the cell surface both by immunolabelling (Zhao et al., 2012), and via the use of a small-molecule fluorescent probe, SR101-F-araNMN (Shrimp et al., 2014). We speculate that the plasma membrane localization of the zebrafish ARC1-like might involve a glycosylphosphatidylinositol (GPI)-anchor, as has already been suggested for the mouse ARC2 (*Mm*BST1; Kaisho et al., 1994), and sea urchin ARC2 (*Sp*ARC2; Churamani et al., 2008). However, the results from our *in silico* prediction using the PredGPI prediction server (http://gpcr.biocomp.unibo.it/predgpi; Pierleoni et al., 2008), suggested a low probability (i.e., specificity index of 42.5%) for the presence of a GPI anchor in the zebrafish ARC1-like amino acid sequence. Nonetheless, we suggest that rigorous *in vitro* biochemical assays (Kaisho et al., 1994; Churamani et al., 2008), are required to test the possible involvement of a GPI anchor in the plasma membrane localization of zebrafish ARC1-like.

Interestingly, we also showed the localization of ARC1-like-EGFP in the acidic vesicles (Figs. 3Bi, 3Bii and 3B*), Golgi complex (Figs. 3Ci, 3Cii and 3C*), and SR (Figs. 3Di, 3Dii and 3D*). We have previously reported that in slow muscle cells, both TPC2 and acidic vesicles are expressed in distinct striated patterns (perpendicular to the long axis of the myofibril), which are associated with the sarcomeric I-bands and Z-lines (see Figs. 3 and 4 of Kelu et al, 2015). This striated pattern of acidic vesicles along the length of an individual myofibril is also clear in Fig. 3B*, where the acidic vesicle labeling overlaps with that of ARC1-like-EGFP. It would appear, therefore, in the case of zebrafish slow muscle cells that the site of endogenous agonist (i.e., NAADP) production, as well as the channel targeted by the agonist (i.e., TPC2) are both localized on (or near) acidic vesicles, which are themselves

distributed in a highly localized manner that reflects their hypothesized function of triggering more global signals via Ca^{2+} release from the SR (Patel et al., 2010; Zhu et al., 2010; Guo et al., 2017). A somewhat similar situation has been shown in oocytes of the sea star *Patitria miniata* where TPCs have been reported to be localized in the internal membranes of cortical granules, and *Pm*ARC, is found in nearby vesicles in the egg cortex (Ramos et al., 2014). This is another example of the endogenous agonist being synthesized close to the target channel. Furthermore, the capability of lysosome-residing CD38 to catalyze the synthesis of NAADP was recently demonstrated in human LP-1 cells (Fang et al., 2018). It was shown that endogenously-expressed surface CD38 was naturally and continuously delivered to the endolysosomal system via endocytosis, and the endolysosomal CD38 was stable and enzymatically active (Fang et al., 2018). As the base-exchange reaction requires an acidic pH (Aarhus et al., 1995), it was thus suggested that the delivery of CD38 into acidic compartments might provide a favorable environment for NAADP production (Lee, 2012; Galione, 2015).

The specific localization of ARC in the Golgi complex and the E/SR has also previously been reported. With regards to the former, endogenous CD38 was observed to localize in the Golgi complex in the rat cerebellar cortex, as revealed by immunolabelling (Yamada et al., 1997). Moreover, an overexpressed human CD38-EGFP was also seen to localize in the Golgi complex in J77 Jurkat cells (Muñoz et al., 2008). In the case of overexpressed ARCs, their presence in the Golgi complex might be a result of a cell attempting to deal with the excess expression of a protein (Baneyx and Mujacic, 2004; Kincaid and Cooper, 2007). This argument, however, does not hold for endogenous ARCs, suggesting that they do have a role associated with Golgi function. With regards to the E/SR, an overexpressed sea urchin ARC1 was seen to localize in the ER of *Xenopus* oocytes and eggs, as well as in HEK cells (Churamani et al., 2007), and endogenous CD38 was observed to localize in the SR of both mouse and rabbit primary ventricular myocytes as revealed by immunolabelling (Lin et al., 2017).

Our study of ARC1-like revealed a heterogeneous localization pattern in primary cultured slow muscle cells. This is somewhat similar to a previous study conducted using mouse MC3T3-E1 osteoblastic cells, where an overexpressed rabbit CD38-EGFP was observed to localize in multiple cellular compartments, including the plasma membrane, Golgi complex, and ER (Sun et al., 2002). Importantly, such heterogeneous localization was recapitulated by the endogenous CD38 in the same study (Sun et al., 2002). In addition, using immunostaining, endogenous ARC2-3 was shown to localize in the acidic vesicles (i.e., cortical granules) in sea urchin eggs; whereas endogenous ARC1 was localized ectocellularly (Davis et al., 2008). Moreover, an overexpressed rat CD38-EGFP was seen to localize both in the plasma membrane and in endolysosomes in mouse pancreatic acinar cells (Cosker et al., 2010).

ARCs have also been reported to be localized in the nuclear envelop or within the nucleus (Adebanjo et al., 1999; Bezin et al., 2008). This was not fully investigated in our current zebrafish study as a nuclear marker was not employed; however, it is clear from Figs. 3Bi and 3Bii, that there is considerable amount of ARC1-like-EGFP and acidic vesicles (using LysoTracker Red DND-99) around what appears to be the nucleus (indicated by "N?" in Figs. 3Bi and 3Bii). This labeling closely resembles the LAMP1 (acidic vesicle) and TPC2 peri-nuclear labeling shown in Figs. 5A to 5D of Kelu et al (2015), suggesting that the ARC1-like-EGFP is indeed peri-nuclear in this slow muscle cell. Our ARC1-like-EGFP data are also supported by electrophysiological evidence for functional TPC2 in the nuclear membrane (Lee et al., 2016).

It has previously been suggested that CD38 is required for the establishment of the anterior-posterior axis and the gross development of skeletal muscle in *Xenopus* embryos (Churamani et al., 2012). Using a bipartite approach, i.e., pharmacological inhibition via nicotinamide (Fig. 4) and molecular knockdown via *ARC1-like*-MO-S (Figs 5 and S3), we showed that ARC activity and *arc1-like* expression are both necessary for the patterning of the myotome and the formation of the sarcomeres in zebrafish slow muscle cells. Indeed, the nicotinamide treatment and ARC1-like-knockdown appeared to phenocopy the previously reported bafilomycin A1-/ *trans*-ned-19-treatment, and TPC2-knockdown/ -knockout with respect to slow muscle cell development (Kelu et al., 2015; 2017). Our data also support a previous report suggesting a role of NAADP/TPC2/Ca^{2+} signaling during the differentiation of myoblasts *in vitro* (Aley et al., 2010). Furthermore, we observed that in the ARC1-like morphants, the mortality rate increased in a dose-dependent manner (Fig. S3); where development frequently stopped during gastrulation, after which these embryos lysed. A somewhat similar result was observed in sea star embryos using an *ARC*-MO (Ramos et al., 2014).

Importantly, we showed that the NAADP level was reduced by ~50% after the nicotinamide treatment (Fig. 4Gi); this suggests that the defects in slow muscle cell development might be due to a lack of NAADP-mediated Ca^{2+} release. It has previously been suggested that nicotinamide forces the base-exchange reaction of ARC in the reverse direction, and thus decreases the rate of NAADP synthesis when it is present in excess (i.e., at millimolar concentrations; Chini, 2009; Churamani et al., 2012; Lin et al., 2017). Although we cannot rule out the possibility that the high concentration of nicotinamide used might cause off-targeting effect(s), our data suggest that when used at 50 mM, nicotinamide is at least effective in inhibiting ARC activity with respect to NAADP synthesis (Fig. 4Gi). In addition, we showed that the production of NAADP was not altered when embryos were treated with 50 mM benzamide (Fig. 4Gii). This suggests that application of a chemical (i.e., benzamide) that is structurally similar to nicotinamide, did not affect NAADP production, which indicates the structural selectivity of nicotinamide in the inhibition of the base-exchange reaction. As ARC1-like is the only

ARC homolog identified in zebrafish so far (Table 1, Figs. 1, S1), we therefore propose that this might be the enzyme responsible for supporting the cyclase activity and base-exchange reaction (i.e., NAADP synthesis) in zebrafish embryos during slow muscle development. However, the capability of ARC1-like to generate NAADP requires further investigation.

In addition to NAADP, ARCs have also been suggested to generate the Ca^{2+} mobilizing messenger cADPR, which targets ryanodine receptors (RyRs) located on the E/SR (Lee, 2011; 2012). The role of the cADPR or RyR in mediating the Ca^{2+} signaling during the differentiation and function of skeletal muscle cells have previously been reported (Brennan et al., 2005; Cheung et al., 2011; Park et al., 2018). Thus, it is possible that following ARC1-like-inhibition or knockdown, the defects in slow muscle cell development observed, might be due to a combinatorial effect of the loss of both cADPR/RyR/Ca^{2+} signaling and NAADP/TPC2/Ca^{2+} signaling. Indeed, we showed that the frequency and amplitude of the Ca^{2+} transients generated in slow muscle cells were both decreased after either ARC1-like-knockdown (Fig. 6) or nicotinamide treatment (Fig. S4).

Our new data therefore might suggest that the ARC1-like/NAADP/TPC2/Ca^{2+} signaling pathway plays a role during slow muscle development. Even though the regulation of ARC activity (and hence the production of NAADP) during slow muscle development is currently not known, we speculate that this might somehow be linked with excitation-contraction coupling. We have previously shown that the inhibition of neural action potentials inhibited the pattern of Ca^{2+} transients generated in the primary motor neurons and led to the attenuation of NAADP production (Kelu et al., 2018). We therefore suggest that during the spontaneous coiling activity of zebrafish embryos (Saint-Amant and Drapeau, 1998), action potentials from the primary motor neurons depolarize the sarcolemma, which activates the membrane-bound ARC1-like (Fig. 3) and leads to the production of NAADP (Kelu et al., 2018). The NAADP in turn targets TPC2 to mediate the release of Ca^{2+} from the slow muscle cells, and these Ca^{2+} signals are required for initiating a myogenic transcriptional program in zebrafish *in vivo* (Kelu et al., 2015; 2017). However, the details of the precise molecular mechanism utilized by zebrafish ARC1-like to synthesize both cADPR and NAADP require further investigation.

ACKNOWLEDGMENTS

We thank Philip Ingham (University of Exeter, UK) for providing us with the smyhc1;GCaMP3 transgenic fish, Grant Churchill (University of Oxford, UK) for teaching JJK the NAADP cycling assay, and Antony J. Morgan (University of Oxford, UK) for discussing the structural resemblance between nicotinamide and benzamide.

COMPETING INTERESTS

The authors declare that they have no competing interests with the contents of this article.

FUNDING

This work was funded by the HK RGC General Research Fund awards 16101714 and 16100115. We also acknowledge funding from the HKITC (ITCPD/17-9), and an HKUST Overseas Research Award for JJK to work with AG. AG is a Wellcome Trust Senior Investigator.

REFERENCES

Aarhus, R., Graeff, R.M., Dickey, D.M., Walseth, T.F., and Lee, H.C. (1995). ADP-ribosyl cyclase and CD38 catalyze the synthesis of a calcium-mobilizing metabolite from NADP. *J. Biol. Chem.* **270**:30327-30333.

Adebanjo, O.A., Anandatheerthavarada, H.K., Koval, A.P., Moonga, B.S., Biswas, G., Sun, L., Sodam, B.R., Bevis, P.J., Huang, C.L.H., Epstein, S., Lai, F.A., Avadhani, N.G., and Zaidi, M. (1999). A new function for CD38/ADP-ribosyl cyclase in nuclear Ca^{2+} homeostasis. *Nat. Cell Biol.* **1**:409-414.

Aley, P.K., Mikolajczyk, A.M., Munz, B., Churchill, G.C., Galione, A., and Berger, F., (2010). Nicotinic acid adenine dinucleotide phosphate regulates skeletal muscle differentiation via action at two-pore channels. *Proc. Natl. Acad. Sci. U.S.A.* **107**:19927-19932.

Baneyx, F., and Mujacic, M. (2004). Recombinant protein folding and misfolding in *Escherichia coli*. *Nat. Biotech.* **22**:1399-1408.

Berridge, M.J. (2012). Calcium signaling, remodelling and disease. *Biochem. Soc. Trans.* **40**:297-309.

Bezin, S., Charpentier, G., Lee, H.C., Baux, G., Fossier, P., and Cancela, J.M. (2008). Regulation of nuclear Ca^{2+} signaling by translocation of the Ca^{2+} messenger synthesizing enzyme ADP-ribosyl cyclase during neuronal depolarization. *J. Biol. Chem.* **283**:27859-27870.

Brennan, C., Mangoli, M., Dyer, C.E., and Ashworth, R. (2005). Acetylcholine and calcium signaling regulate muscle fiber formation in the zebrafish embryo. *J. Cell Sci.* **118**:5181-5190.

Calcraft, P.J., Ruas, M., Pan, Z., Cheng, X., Arredouani, A., Hao, X., Tang, J., Rietdorf, K., Teboul, L., Chuang, K-T., Lin, P., Xiao, R., Wang, C., Zhu, Y., Lin, Y., Wyatt, C.N., Parrington, J., Ma, J., Evans, A.M., Galione, A., and Zhu, M.X. (2009). NAADP mobilizes calcium from acidic organelles through two-pore channels. *Nature* **459**:596-600.

Cheung, C.Y., Webb, S.E., Love, D.R., and Miller, A.L., (2011). Visualization, characterization and modulation of calcium signaling during the development of slow muscle cells in intact zebrafish embryos. *Int. J. Dev. Biol.* **55**:153-174.

Cheung, C.Y., Webb, S.E., Meng, A., and Miller, A.L. (2006). Transient expression of apoaequorin in zebrafish embryos: extending the ability to image calcium transients during later stages of development. *Int. J. Dev. Biol.* **50**:561-569.

Chini, E.N. (2009). CD38 as a regulator of cellular NAD: a novel potential pharmacological target for metabolic conditions. *Curr. Pharm. Des.* **15**:57-63.

Churamani, D., Boulware, M.J., Geach, T.J., Martin, A.C., Moy, G.W., Su, Y.H., Vacquier, V.D., Marchant, J.S., Dale, L., and Patel, S. (2007). Molecular characterization of a novel intracellular ADP-ribosyl cyclase. *PLoS One* **2**:e797. https://doi.org/10.1371/journal.pone.0000797

Churamani, D., Geach, T.J., Ramakrishnan, L., Prideaux, N., Patel, S., and Dale, L., (2012). The signaling protein CD38 is essential for early embryonic development. *J. Biol. Chem.* **287**:6974-6978.

Churchill, G.C., Okada, Y., Thomas, J.M., Genazzani, A.A., Patel, S., and Galione, A. (2002). NAADP mobilizes Ca^{2+} from reserve granules, lysosome-related organelles, in sea urchin eggs. *Cell* **111**:703-708.

Cosker, F., Cheviron, N., Yamasaki, M., Menteyne, A., Lund, F.E., Moutin, M.J., Galione, A., and Cancela, J.M. (2010). The ecto-enzyme CD38 is a nicotinic acid adenine dinucleotide phosphate (NAADP) synthase that couples receptor activation to Ca^{2+} mobilization from lysosomes in pancreatic acinar cells. *J. Biol. Chem.* **285**:38251-38259.

Davis, L.C., Morgan, A.J., Ruas, M., Wong, J.L., Graeff, R.M., Poustka, A.J., Lee, H.C., Wessel, G.M., Parrington, J., and Galione, A. (2008). Ca^{2+} signaling occurs via second messenger release from intraorganelle synthesis sites. *Curr. Biol.* **18**:1612-1618.

Deshpande, D.A., White, T.A., Guedes, A.G., Milla, C., Walseth, T.F., Lund, F.E., and Kannan, M.S. (2005). Altered airway responsiveness in CD38-deficient mice. *Am. J. Respir. Cell Mol. Biol.* **32**:149-156.

Fang, C., Li, T., Li, Y., Xu, G.J., Deng, Q.W., Chen, Y.J., Hou, Y.N., Lee, H.C., and Zhao, Y.J. (2018). CD38 produces nicotinic acid adenosine dinucleotide phosphate in the lysosome. *J. Biol. Chem.* **293**:8151-8160.

Ferrero, E., Lo Buono, N., Horenstein, A.L., Funaro, A., and Malavasi, F. (2014). The ADP-ribosyl cyclases-the current evolutionary state of the ARCs. *Front. Biosci. (Landmark Ed)* **19**:986-1002.

Galione, A. (2015). A primer of NAADP-mediated Ca^{2+} signalling: From sea urchin eggs to mammalian cells. *Cell Calcium* **58**:27-47.

Graeff, R.M., and Lee, H.C. (2013). An improved enzymatic cycling assay for NAADP. *Messenger* **2**:96-105.

Guo, J., Zeng, W., and Jiang, Y. (2017). Tuning the ion selectivity of two-pore channels. *Proc. Natl. Acad. Sci. USA* **114**:1009-1014.

Guse, A.H., and Diercks, B.P. (2018). Integration of nicotinic acid adenine dinucleotide phosphate (NAADP)-dependent calcium signalling. *J. Physiol.* **596**:2735-2743.

Higashida, H., Liang, M., Yoshihara, T., Akther, S., Fakhrul, A., Stanislav, C., Nam, T.S., Kim, U.H., Kasai, S., Nishimura, T., Al Mahmuda, N., Yokoyama, S., Ishihara, K., Gerasimenko, M., Salmina, A., Zhong, J., Tsuji, T., Tsuji, C., and Lopatina, O. (2017). An immunohistochemical, enzymatic, and behavioral study of CD157/BST-1 as a neuroregulator. *BMC Neurosci.* **18**:35. Doi: 10.1186/s12868-017-0350-7.

Howard, M., Grimaldi, J.C., Bazan, J.F., Lund, F.E., Santos-Argumedo, L., Parkhouse, R.M., Walseth, T.F., and Lee, H.C. (1993). Formation and hydrolysis of cyclic ADP-ribose catalyzed by lymphocyte antigen CD38. *Science* **262**:1056-1059.

Itoh, M., Ishihara, K., Tomizawa, H., Tanaka, H., Kobune, Y., Ishikawa, J., Kaisho, T., and Hirano, T. (1994). Molecular cloning of murine BST-1 having homology with CD38 and *Aplysia* ADP-ribosyl cyclase. *Biochem. Biophys. Res. Commun.* **203**:1309-1317.

Jackson, D.G., and Bell, J.I. (1990). Isolation of a cDNA encoding the human CD38 (T10) molecule, a cell surface glycoprotein with an unusual discontinuous pattern of expression during lymphocyte differentiation. *J. Immunol.* **144**:2811-2815.

Jackson, H.E., and Ingham, P.W. (2013). Control of muscle fibre-type diversity during embryonic development: The zebrafish paradigm. *Mech. Dev.* **130**:447-457.

Jackson, H.E., Ono, Y., Wang, X., Elworthy, S., Cunliffe, V.T., and Ingham, P.W. (2015). The role of Sox6 in zebrafish muscle fiber type specification. *Skeletal Muscle* **5**:2. Doi: 10.1186/s13395-014-0026-2

Jha, A., Ahuja, M., Patel, S., Brailoiu, E., and Muallem, S. (2014). Convergent regulation of the lysosomal two-pore channel-2 by Mg^{2+}, NAADP, $PI(3,5)P_2$ and multiple protein kinases. *EMBO J.* **33**:501-511.

Kaisho, T., Ishikawa, J., Oritani, K., Inazawa, J., Tomizawa, H., Muraoka, O., Ochi, T., and Hirano, T. (1994). BST-1, a surface molecule of bone marrow stromal cell lines that facilitates pre-B-cell growth. *Proc. Natl. Acad. Sci. U.S.A.* **91**:5325-5329.

Kelu, J.J., Chan, H.L., Webb, S.E., Cheng, A.H., Ruas, M., Parrington, J., Galione, A., and Miller, A.L. (2015). Two-pore channel 2 activity is required for slow muscle cell-generated Ca^{2+} signaling during myogenesis in intact zebrafish. *Int. J. Dev. Biol.* **59**:313-325.

Kelu, J.J., Webb, S.E., Parrington, J., Galione, A., and Miller, A.L. (2017). Ca^{2+} release via two-pore channel type 2 (TPC2) is required for slow muscle cell myofibrillogenesis and myotomal patterning in intact zebrafish embryos. *Dev. Biol.* **425**:109-129.

Kelu, J.J., Webb, S.E., Galione, A., and Miller, A.L. (2018). TPC2-mediated Ca^{2+} signaling is required for the establishment of synchronized activity in developing zebrafish primary motor neurons. *Dev. Biol.* **438**:57-68.

Kincaid, M.M., and Cooper, A.A. (2007). Misfolded proteins traffic from the endoplasmic reticulum (ER) due to ER export signals. *Mol. Biol. Cell* **18**:455-463.

Lee, C.S.K., Tong, B.C.K., Cheng, C.W.H., Hung, H.C.H., and Cheung, K.H. (2016). Characterization of two-pore channel 2 by nuclear membrane electrophysiology. *Sci. Reports* **6**:20282 DOI: 10.1038/srep20282

Lee, H.C. (2011). Cyclic ADP-ribose and NAADP: fraternal twin messengers for calcium signaling. *Sci. China Life Sci.* **54**:699-711.

Lee, H.C. (2012). Cyclic ADP-ribose and nicotinic acid adenine dinucleotide phosphate (NAADP) as messengers for calcium mobilization. *J. Biol. Chem.* **287**:31633-31640.

Lee, H.C., and Aarhus, R. (1991). ADP-ribosyl cyclase: an enzyme that cyclizes NAD^+ into a calcium-mobilizing metabolite. *Cell Regul.* **2**:203-209.

Lin, W.K., Bolton, E.L., Cortopassi, W.A., Wang, Y., O'Brien, F., Maciejewska, M., Jacobson, M.P., Garnham, C., Ruas, M., Parrington, J., Lei, M., Sitsapesan, R., Galione, A., and Terrar, D.A. (2017). Synthesis of the Ca^{2+}-mobilizing messengers NAADP and cADPR by intracellular CD38 enzyme in the mouse heart: Role in β-adrenoceptor signaling. *J. Biol. Chem.* **292**:13243-13257.

Lin-Moshier, Y., Walseth, T.F., Churamani, D., Davidson, S.M., Slama, J.T., Hooper, R., Brailoiu, E., Patel, S., Marchant, J.S. (2012). Photoaffinity labeling of nicotinic acid adenine dinucleotide phosphate (NAADP) targets in mammalian cells. *J. Biol. Chem.* **287**:2296-2307.

Liu, Q., Kriksunov, I.A., Graeff, R., Munshi, C., Lee, H.C., and Hao, Q. (2005). Crystal structure of human CD38 extracellular domain. *Structure* **13**:1331-1339.

Liu, Q., Kriksunov, I.A., Graeff, R., Munshi, C., Lee, H.C., and Hao, Q. (2006). Structural basis for the mechanistic understanding of human CD38-controlled multiple catalysis. *J. Biol. Chem.* **281**:32861-32869.

Mészáros, L.G., Bak, J., and Chu, A. (1993). Cyclic ADP-ribose as an endogenous regulator of the non-skeletal type ryanodine receptor Ca^{2+} channel. *Nature* **364**:76-79.

Morcos, P.A. (2007). Achieving targeted and quantifiable alteration of mRNA splicing with Morpholino oligos. *Biochem. Biophys. Res. Commun.* **358**:521-527.

Muñoz, P., Mittelbrunn, M., de la Fuente, H., Pérez-Martínez, M., García-Pérez, A., Ariza-Veguillas, A., Malavasi, F., Zubiaur, M., Sánchez-Madrid, F., and Sancho, J. (2008). Antigen-induced clustering of surface CD38 and recruitment of intracellular CD38 to the immunologic synapse. *Blood* **111**:3653-3664.

Munshi, C., Thiel, D.J., Mathews, I.I., Aarhus, R., Walseth, T.F., and Lee, H.C. (1999). Characterization of the active site of ADP-ribosyl cyclase. *J. Biol. Chem.* **274**:30770-30777.

Palade, P. (2007). The hunt for an alternate way to generate NAADP. Focus on "NAADP as a second messenger: neither CD38 nor base-exchange reaction are necessary for *in vivo* generation of NAADP in myometrial cells". *Am. J. Physiol. Cell Physiol.* **292**:C4-C7.

Park, D.R., Nam, T.S., Kim, Y.W., Lee, S.H., and Kim, U.H. (2018). CD38-cADPR-SERCA signaling axis determines skeletal muscle contractile force in response to β-adrenergic stimulation. *Cell Physiol. Biochem.* **46**:2017-2030.

Patel, S., Marchant, J., and Brailoiu, E. (2010). Two-pore channels: Regulation by NAADP and customized roles in triggering calcium signals. *Cell Calcium* **47**:480-490.

Pierleoni, A., Martelli, P.L., and Casadio, R. (2008). PredGPI: a GPI-anchor predictor. *BMC Bioinformatics* **9**:392.

Plazas, P.V., Nicol, X., and Spitzer, N.C. (2013). Activity-dependent competition regulates motor neuron axon pathfinding via PlexinA3. *Proc. Natl. Acad. Asci. USA* **110**:1524-1529.

Prasad, G.S., McRee, D.E., Stura, E.A., Levitt, D.G., Lee, H.C., and Stout, C.D. (1996). Crystal structure of *Aplysia* ADP ribosyl cyclase, a homologue of the bifunctional ectozyme CD38. *Nat. Struct. Biol.* **3**:957-964.

Rah, S.Y., Mushtaq, M., Nam, T.S., Kim, S.H., and Kim, U.H. (2010). Generation of cyclic ADP-Ribose and nicotinic acid adenine dinucleotide phosphate by CD38 for Ca^{2+} signaling in interleukin-8-treated lymphokine-activated killer cells. *J. Biol. Chem.* **285**:21877-21887.

Ramakrishnan, L., Muller-Steffner, H., Bosc, C., Vacquier, V.D., Schuber, F., Moutin, M.J., Dale, L., and Patel, S. (2010). A single residue in a novel ADP-ribosyl cyclase controls production of the calcium-mobilizing messengers cyclic ADP-ribose and nicotinic acid adenine dinucleotide phosphate. *J. Biol. Chem.* **285**:19900-19909.

Ramos, I., Reich, A., and Wessel, G.M. (2014). Two-pore channels function in calcium regulation in sea star oocytes and embryos. *Development* **141**:4598-4609.

Robu, M.E., Larson, J.D., Nasevicius, A., Beiraghi, S., Brenner, C., Farber, S.A., and Ekker, S.C. (2007). p53 activation by knockdown technologies. *PLoS Genet.* **3**:e78. Doi: 10.1371/journal.pgen.0030078

Ruas, M., Davis, L.C., Chen, C.C., Morgan, A.J., Chuang, K.T., Walseth, T.F., Grimm, C., Garnham, C., Powell, T., Platt, N., Platt, F.M., Biel, M., Wahl-Schott, C., Parrington, J., and Galione, A. (2015). Expression of Ca^{2+}-permeable two-pore channels rescues NAADP signalling in TPC-deficient cells. *EMBO J.* **34**:1743-1758.

Saint-Amant, L., and Drapeau, P. (1998). Time course of the development of motor behaviors in the zebrafish embryo. *J. Neurobiol.* **37**:622-632.

Schmid, F., Bruhn, S., Weber, K., Mittrücker, H.W., and Guse, A.H. (2011). CD38: a NAADP degrading enzyme. *FEBS Lett.* **585**:3544-3548.

Shrimp, J.H., Hu, J., Dong, M., Wang, B.S., MacDonald, R., Jiang, H., Hao, Q., Yen, A., and Lin, H. (2014). Revealing CD38 cellular localization using a cell permeable, mechanism-based fluorescent small-molecule probe. *J. Am. Chem. Soc.* **136**:5656-5663.

Soares, S., Thompson, M., White, T., Isbell, A., Yamasaki, M., Prakash, Y., Lund, F.E., Galione, A., and Chini, E.N. (2007). NAADP as a second messenger: neither CD38 nor base-exchange reaction

are necessary for *in vivo* generation of NAADP in myometrial cells. *Am. J. Physiol. Cell Physiol.* **292**:C227-C239.

Stainier, D.Y.R., Raz, E., Lawson, N.D., Ekker, S.C., Burdine, R.D., Eisen, J.S., Ingham, P.W., Schulte-Merker, S., Yelon, D., Weinstein, B.M., Mullins, M.C., Wilson, S.W., Ramakrishnan, L., Amacher, S.L., Neuhauss, S.C.F., Meng, A., Mochizuki, N., Panula, P., and Moens, C.B. (2017). Guidelines for morpholino use in zebrafish. *PLoS Genet.* **13**:e1007000. Doi: 10.1371/journal.pgen.1007000

States, D.J., Walseth, T.F., and Lee, H.C. (1992). Similarities in amino acid sequences of *Aplysia* ADP-ribosyl cyclase and human lymphocyte antigen CD38. *Trends Biochem. Sci.* **17**:495. Doi: 10.1016/0968-0004(92)90337-9

Sun, L., Adebanjo, O.A., Koval, A., Anandatheerthavarada, H.K., Iqbal, J., Wu, X.Y., Moonga, B.S., Wu, X.B., Biswas, G., Bevis, P.J.R., Kumegawa, M., Epstein, S., Huang, C.L.-H., Avadhani, N.G., Abe, E., and Zaidi, M. (2002). A novel mechanism for coupling cellular intermediary metabolism to cytosolic Ca^{2+} signaling via CD38/ADP-ribosyl cyclase, a putative intracellular NAD^{+} sensor. *FASEB J.* **16**:302-314.

Vandesompele, J., De Preter, K., Pattyn, F., Poppe, B., Van Roy, N., De Paepe, A., and Speleman, F. (2002). Accurate normalization of real-time quantitative RT-PCR data by geometric averaging of multiple internal control genes. *Genome Biol.* **3**: 0034.

Walseth, T.F., Lin-Moshier, Y., Jain, P., Ruas, M., Parrington, J., Galione, A., Marchant, J.S., and Slama, J.T. (2012). Photoaffinity labeling of high affinity nicotinic acid adenine dinucleotide phosphate (NAADP)-binding proteins in sea urchin egg. *J. Biol. Chem.* **287**:2308-2315.

Waterhouse, A.M., Procter, J.B., Martin, D.M., Clamp, M., and Barton, G.J. (2009). Jalview Version 2 - a multiple sequence alignment editor and analysis workbench. *Bioinform.* **25**:1189-1191.

Westerfield, M. (2000). In *The Zebrafish Book. A Guide for the Laboratory Use of Zebrafish (Danio rerio)* (ed. Westerfield, M.). University of Oregon Press, Eugene.

Yamada, M., Mizuguchi, M., Otsuka, N., Ikeda, K., and Takahashi, H. (1997). Ultrastructural localization of CD38 immunoreactivity in rat brain. *Brain Res.* **756**:52-60.

Yamamoto-Katayama, S., Ariyoshi, M., Ishihara, K., Hirano, T., Jingami, H., and Morikawa, K. (2002). Crystallographic studies on human BST-1/CD157 with ADP-ribosyl cyclase and NAD glycohydrolase activities. *J. Mol. Biol.* **316**:711-723.

Zhao, Y.J., Lam, C.M.C., and Lee, H.C. (2012). The membrane-bound enzyme CD38 exists in two opposing orientations. *Sci Signal* **5**:ra67. Doi: 10.1126/scisignal.2002700

Zhu, M.X., Evans, A.M., Ma, J., Parrington, J., and Galione, A. (2010). Two-pore channels for integrative Ca^{2+} signaling. *Comm. Int. Biol.* **3**:12-17.

Table 1. Homology of ARC across species

	***Hs*CD38**	***Hs*BST1**	***Mm*CD38**	***Mm*BST1**	***Dr*ARC1 -like**	***Sp*ARC1**	***Sp*ARC2**	***Sp*ARC3**	***Sp*ARC4**
***Hs*CD38**		43	73	52	**55**	35	35	33	34
***Hs*BST1**	30		56	86	**53**	44	41	39	39
***Mm*CD38**	59	38		55	**55**	31	46	47	51
***Mm*BST1**	35	75	36		**51**	46	44	49	55
***Dr*ARC1 -like**	**34**	**37**	**34**	**36**		**45**	**42**	**45**	**48**
***Sp*ARC1**	20	26	28	30	**30**		66	34	29
***Sp*ARC2**	22	26	29	27	**26**	51		38	41
***Sp*ARC3**	19	23	27	28	**31**	22	20		38
***Sp*ARC4**	23	22	31	31	**30**	24	25	22	

% Identity
% Similarity

Key: *Homo sapiens* (*Hs*) = Human; *Mus musculus* (*Mm*) = Mouse; *Danio rerio* (*Dr*) = Zebrafish; *Strongylocentrotus purpuratus* (*Sp*) = Purple sea urchin

FIGURE LEGENDS

Fig. 1. Multiple protein sequence alignment diagram prepared using Jalview. Aligned sequences of the ARC homologs were arranged in rows and placed into a single reference frame, where each aligned position occupies a column in the table. The dashed lines indicate gaps. The label on the left side of each sequence provides its name, and the start and end positions are shown at the end of each row. Residues in the alignment are shaded using a graduated color scheme, where the lowest and highest percentage of identity are shaded in "white" and "dark blue", respectively. The histograms below each block of sequences show the "conservation score" for each column of the alignment diagram. The conservation score is based on an 11-point grading scale, i.e., from 0-9 and then "+" and "*", where 0 and "*" indicate the weakest and strongest level of conservation, respectively. Conserved cysteine residues (required for disulphide bond formation) are in yellow; whereas the conserved residues that are important for substrate binding are in red.

Fig. 2. Expression of the *arc1-like* transcript and detection of NAADP in whole zebrafish embryos from ~16 hpf to ~48 hpf. (A) RT-PCR followed by gel electrophoresis was conducted to show the relative expression of *arc1-like* in zebrafish embryos at ~16 hpf, ~18 hpf, ~20 hpf, ~22 hpf, ~24 hpf, and ~48 hpf (n=4 for each time point). β-actin was used as an internal control. **(B)** Bar graph to show the mean ± SEM fold-change in *arc1-like* expression detected by quantitative real-time PCR (qPCR) relative to 16 hpf (n=6). The expression of *arc1-like* was normalized to three house-keeping genes, *actb2*, *ef1α*, and *rpl13a*. **(C)** The NAADP cycling assay was employed to detect the endogenous level of NAADP in whole embryo extracts prepared at ~16 hpf, ~18 hpf, ~20 hpf, ~22 hpf, ~24 hpf, and ~48 hpf. This bar graph shows the normalized [NAADP] detected in the extract samples, and the corresponding fold-change in [NAADP] (n=9). In **(B)** and **(C)**, the asterisks indicate statistically significant differences at $p<0.05$ (*), $p<0.01$ (**) and $p<0.001$ (***). In **(C)**, the data obtained at ~18 hpf to ~48 hpf was compared statistically, with those obtained at ~16 hpf.

Fig. 3. Localization of ARC1-like fusion proteins in zebrafish primary cultured muscle cells. (A-D) Approximately 100-200 ng of either *arc1-like-EGFP* mRNA or *arc1-like-tdTomato* mRNA was injected into the blastodisc of zebrafish embryos at the one-cell stage to transiently overexpress the ARC1-like fusion proteins. At ~48 hpf, the embryos were digested and primary cultures were prepared from the dissociated cells. Primary cultured muscle cells that expressed **(Ai, Bi)** ARC1-like-EGFP were then labeled with **(Aii)** FM 6-46 (n=24) or **(Bii)** LysoTracker Red DND-99 (n=44) to visualize the plasma membrane or acidic vesicles, respectively, whereas those expressing **(Ci, Di)** ARC1-like-tdTomato were labeled with **(Cii)** BODIPY FL C5-ceramide (n=16) or **(Dii)** ER-Tracker Green (n=14) to visualize the Golgi

complex or sarcoplasmic reticulum (SR), respectively. These are single optical sections to show the distribution of **(Ai, Bi)** ARC1-like-EGFP expression (in green) with respect to **(Aii)** the plasma membrane or **(Bii)** acidic vesicles (both in red), or the distribution of **(Ci, Di)** ARC1-like-tdTomato expression (in red) with respect to **(Cii)** the Golgi complex or **(Dii)** the sarcoplasmic reticulum (both in green). The regions bounded by the white squares in panels **(Ai-Aii, Bi-Bii, Ci-Cii, Di-Dii)** are shown at higher magnification and when the green and red channels are merged in the panels **(A*, B*, C*, D*)**, respectively. In the merged images in the panels **(A*-D*)**, overlapping regions are shown in yellow. The arrowheads in panels **(A*-D*)** indicate overlap in fluorescence (yellow) between the ARC1-like fusion proteins and the various cellular compartments. "N?" in panel **(Bi, Bii)** is the putative location of the nucleus. Scale bars, 10 µm (in panels **Ai-Aii, Bi-Bii, Ci-Cii, Di-Dii**); and 2 µm (in panels **A*-D***).

Fig. 4. Effect of nicotinamide on the organization of the trunk musculature and the formation of the sarcomeres. At ~17 hpf, embryos had the terminal portion of the tail excised and then they were treated with **(A)** Danieau's solution alone or Danieau's solution containing nicotinamide at: **(Bi)** 1 mM, **(Bii)** 10 mM, or **(Biii)** 50 mM. All the embryos were fixed at ~24 hpf and dual-labeled with phalloidin and the F59 antibody, to visualize F-actin (in green) and myosin heavy chain (in red) in the trunk musculature, respectively. The panels show series of optical sections projected as single images at **(A, Bi-Biii)** low and **(A*, Bi*-Biii*)** higher magnification when the green and red channels are merged; overlapping regions are shown in yellow. The higher magnification images of the slow myofibers reveal the presence or absence of the sarcomeric banding pattern. The white arrows in panel **(Biii)** show the disorganized nature of some slow myofibers. Ant. and Pos. are anterior and posterior, respectively. Scale bars, 50 µm (in panels **A, Bi-Biii**), and 2 µm (in panels **A*, Bi*-Biii***). **(C-F)** In order to determine the level of disruption on slow muscle cell development following nicotinamide treatment, various dimensions of the trunk musculature and slow myofibers were measured. These bar graphs show the mean ± SEM: **(C)** myotome width (all n=15, from 5 embryos), **(D)** somite angle (n=15, from 5 embryos), **(E)** myofiber length:somite length ratio (n=60 from 5 embryos); and **(F)** myofiber width (n=50, from 5 embryos). The black dashed line in panel **(E)** indicates a myofiber:somite length ratio of 1. **(Gi)** The NAADP cycling assay was employed to detect the endogenous level of NAADP in whole embryo extracts that were either untreated, or treated with nicotinamide or benzamide. This bar graph shows the normalized [NAADP] detected in sample extracts and the corresponding fold-change in [NAADP] (n=3). **(Gii)** Chemical structure of nicotinamide and benzamide. In panels **(C-G)**, the asterisks indicate statistically significant differences at $p<0.05$ (*) and $p<0.001$ (***), whereas NS indicates that no significant difference was observed.

Fig. 5. Effect of MO-based knockdown of ARC1-like (without and with mRNA rescue) on the organization of the trunk musculature and the formation of the sarcomeres. Embryos were injected with **(A)** ~5 ng standard control-MO; **(B)** ~5 ng *p53*-MO; **(Ci)** ~1 ng *ARC1-like*-MO-S + ~1 ng *p53*-MO; **(Cii)** ~2 ng *ARC1-like*-MO-S + ~2 ng *p53*-MO; or **(D)** ~2 ng *ARC1-like*-MO-S + ~2 ng *p53*-MO + ~100 ng *arc1-like* mRNA. All the embryos were fixed at ~24 hpf and dual-labeled with phalloidin and the F59 antibody, to visualize F-actin (in red) and myosin heavy chain (in green) in the trunk musculature, respectively. The panels show a series of optical sections projected as single images at **(A, B, Ci, Cii, D)** low and **(A*, B*, Ci*, Cii*, D*)** higher magnification when the red and green channels are merged; overlapping regions are shown in yellow. The higher magnification images of the slow myofibers reveal the presence or absence of the sarcomeric banding pattern of the F-actin and myosin heavy chain. The white arrows in panels **(Ci, Cii)** show the disorganization of some of the slow myofibers, whereas the white arrow heads in panel **(Cii*)** indicate a fracture in one of the myofibers. Ant. and Pos. are anterior and posterior, respectively. Scale bars, 50 μm (in panels A, B, Ci, Cii, D), and 2 μm (in panels A*, B*, Ci*, Cii*, D*). **(E-H)** In order to determine the level of disruption on slow muscle cell development following ARC1-like-knockdown, various dimensions of the trunk musculature and slow myofibers were measured. These bar graphs show the mean ± SEM: **(E)** myotome width (all n=18, from 6 embryos), **(F)** somite angle (n=18, from 6 embryos), **(G)** myofiber length:somite length ratio (n=162 from 6 embryos); and **(H)** myofiber width (n=60, from 6 embryos). The black dashed line in panel **(G)** indicates a myofiber:somite length ratio of 1. The asterisks indicate statistically significant differences at $p<0.001$ (***), whereas NS indicates that no significant difference was observed.

Fig. 6. Effect of MO-based knockdown of ARC1-like (without and with mRNA rescue) on Ca^{2+} signaling in the slow muscle cells at ~18 hpf and ~24 hpf. Smyhc1:GCaMP3 transgenic embryos were either untreated (controls), or else they were injected with: ~5 ng standard control-MO; ~5 ng *p53*-MO; ~1 ng *ARC1-like*-MO-S + ~1 ng *p53*-MO; ~2 ng *ARC1-like*-MO-S + ~2 ng *p53*-MO; or ~2 ng *ARC1-like*-MO-S + ~2 ng *p53*-MO + ~100 ng *arc1-like* mRNA. **(Ai, Bi)** Representative confocal images showing the GCaMP3 fluorescence in the slow muscle cells in untreated (control) embryos at **(Ai)** ~18 hpf and **(Bi)** ~24 hpf. The embryos are in a lateral orientation and the red rectangles show regions of interest (ROI), which were placed on a selected slow muscle cell. The black dashed lines show the location of the vertical myosepta. Ant. and Pos. are anterior and posterior, respectively. Scale bar, 50 μm. **(Aii, Bii)** Representative line graphs showing the $\Delta F/F_0$ against time (over a period of ~180 sec) in the ROIs on selected slow muscle cells in the various treatment groups at **(Aii)** ~18 hpf and **(Bii)** ~24 hpf. **(Aiii, Biii)** Bar graphs to show the mean ± SEM frequency of the Ca^{2+} transients at **(Aiii)** ~18 hpf and **(Biii)**

~24 hpf. **(Aiv, Biv)** Bar graphs to show the mean ± SEM amplitude of the Ca^{2+} transients at **(Aiv)** ~18 hpf and **(Biv)** ~24 hpf. In **(Aiii, Aiv)**, n=15-25, from 3-5 embryos, and in **(Biii, Biv)**, n=25-30, from 5-6 embryos. **(C)** Bar graphs to compare the mean ± SEM **(Ci)** frequency and **(Cii)** amplitude of the Ca^{2+} transients at 18 hpf and 24 hpf. In panels **(Aiii, Aiv, Biii, Biv, Ci, Cii)**, the asterisks indicate statistically significant differences at $p<0.05$ (*), $p<0.01$ (**) and $p<0.001$ (***), whereas NS indicates that no significant difference was observed.

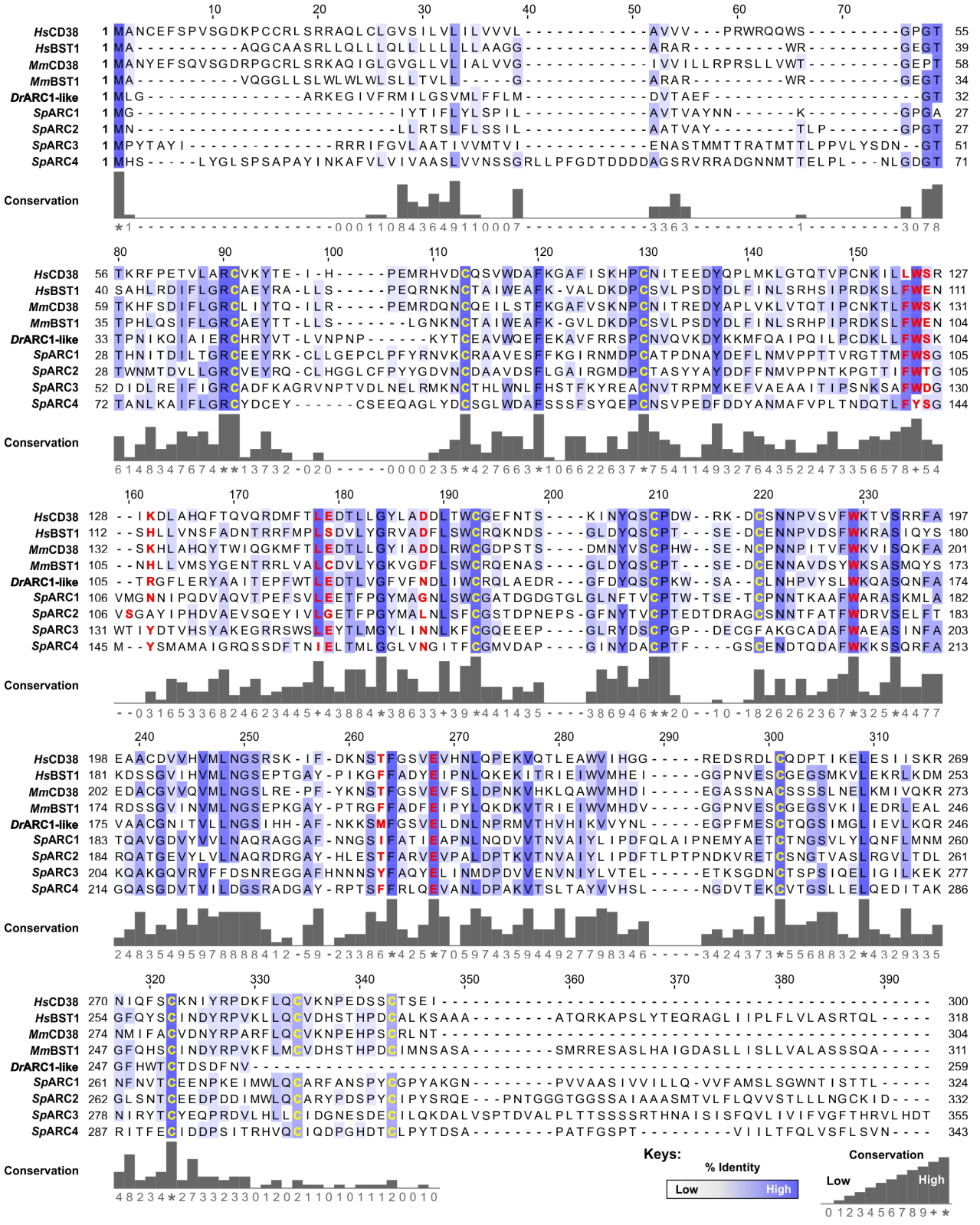
HsCD38
HsBST1
MmCD38
MmBST1
DrARC1-like
SpARC1
SpARC2
SpARC3
SpARC4
Conservation
Keys:
% Identity
Low
High
Conservation
Low
High

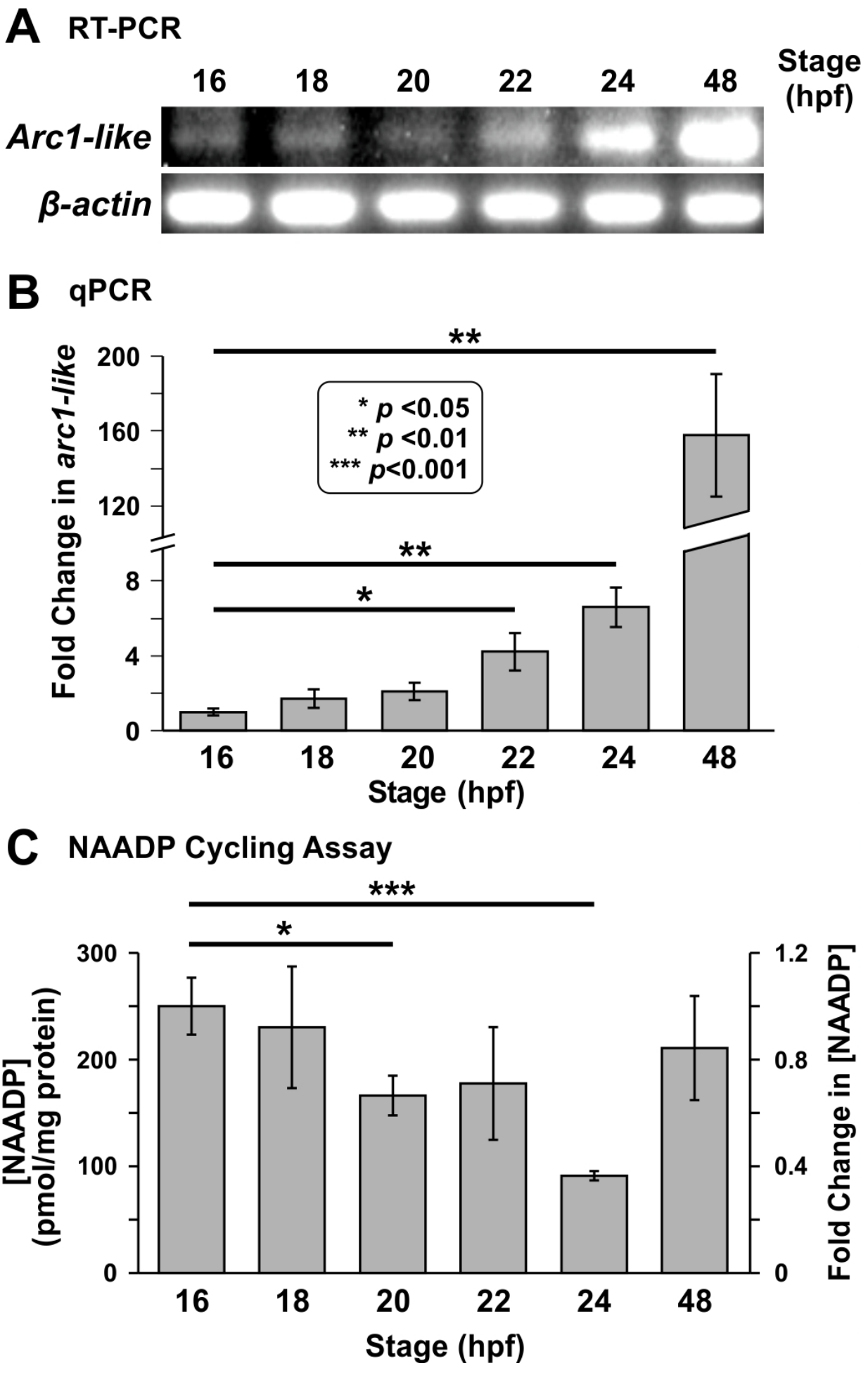
A RT-PCR
16
18
20
22
24
48
Stage (hpf)
Arc1-like
β-actin
B qPCR
**
* p <0.05
** p <0.01
*** p<0.001
**
*
Fold Change in arc1-like
200
160
120
8
4
0
16
18
20
22
24
48
Stage (hpf)
C NAADP Cycling Assay
***
*
[NAADP] (pmol/mg protein)
300
200
100
0
1.2
0.8
0.4
0
Fold Change in [NAADP]
16
18
20
22
24
48
Stage (hpf)

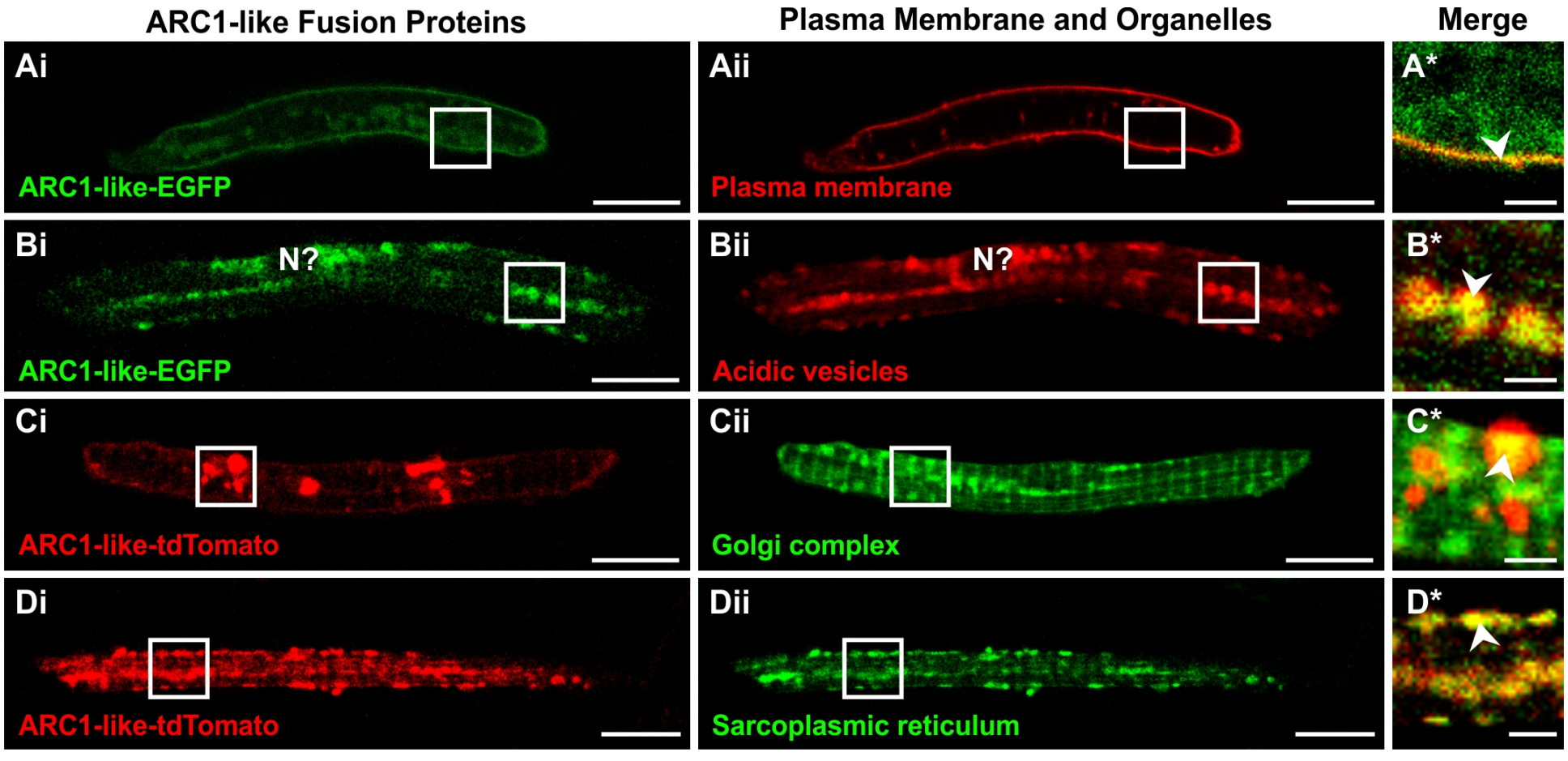
ARC1-like Fusion Proteins
Plasma Membrane and Organelles
Merge
Ai
ARC1-like-EGFP
Aii
Plasma membrane
A*
Bi
N?
ARC1-like-EGFP
Bii
N?
Acidic vesicles
B*
Ci
ARC1-like-tdTomato
Cii
Golgi complex
C*
Di
ARC1-like-tdTomato
Dii
Sarcoplasmic reticulum
D*

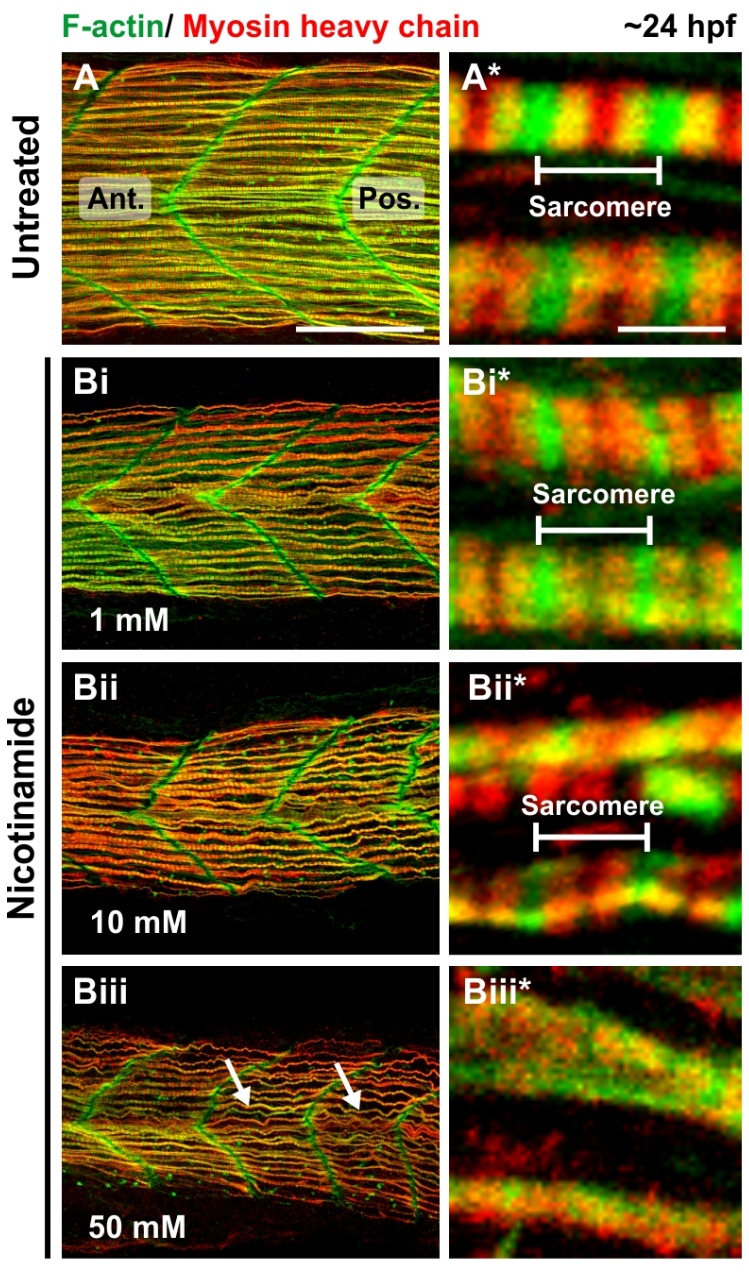
F-actin/ Myosin heavy chain
~24 hpf
Untreated
Nicotinamide
A
A*
Ant.
Pos.
Sarcomere
Bi
Bi*
1 mM
Bii
Bii*
10 mM
Biii
Biii*
50 mM

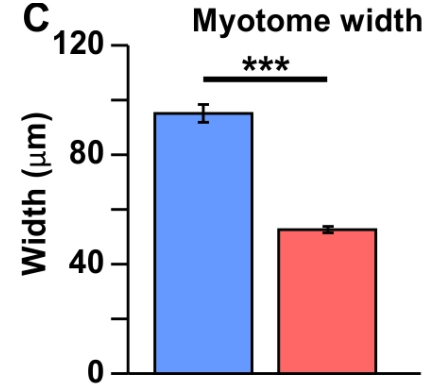
C
Myotome width
***
Width (μm)
120
80
40
0

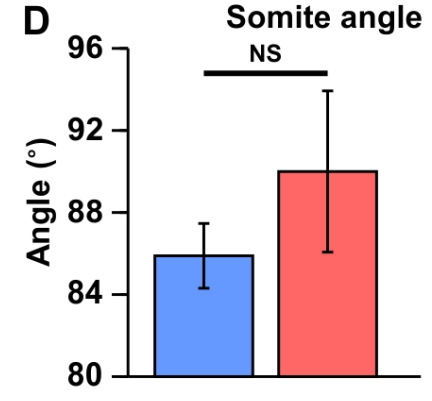
D
Somite angle
NS
Angle (°)
96
92
88
84
80

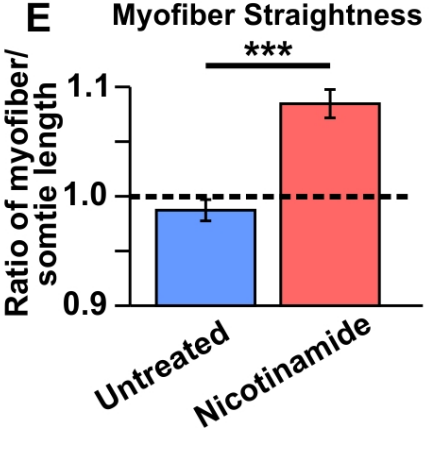
E
Myofiber Straightness
***
Ratio of myofiber/ somtie length
1.1
1.0
0.9
Untreated
Nicotinamide

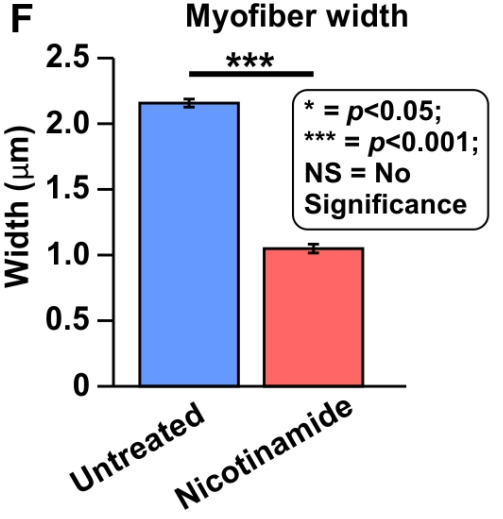
F
Myofiber width
***
* = p<0.05;
*** = p<0.001;
NS = No Significance
Width (μm)
2.5
2.0
1.5
1.0
0.5
0
Untreated
Nicotinamide

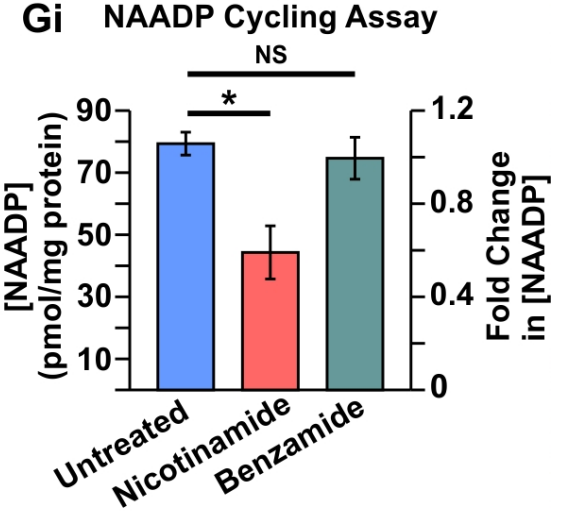
Gi
NAADP Cycling Assay
NS
*
[NAADP] (pmol/mg protein)
90
70
50
30
10
1.2
0.8
0.4
0
Fold Change in [NAADP]
Untreated
Nicotinamide
Benzamide

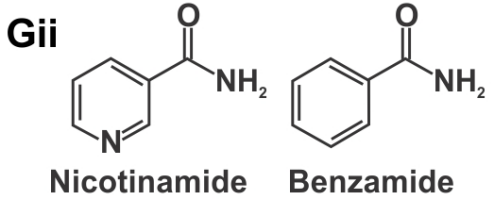
Gii
O
NH2
N
Nicotinamide
Benzamide

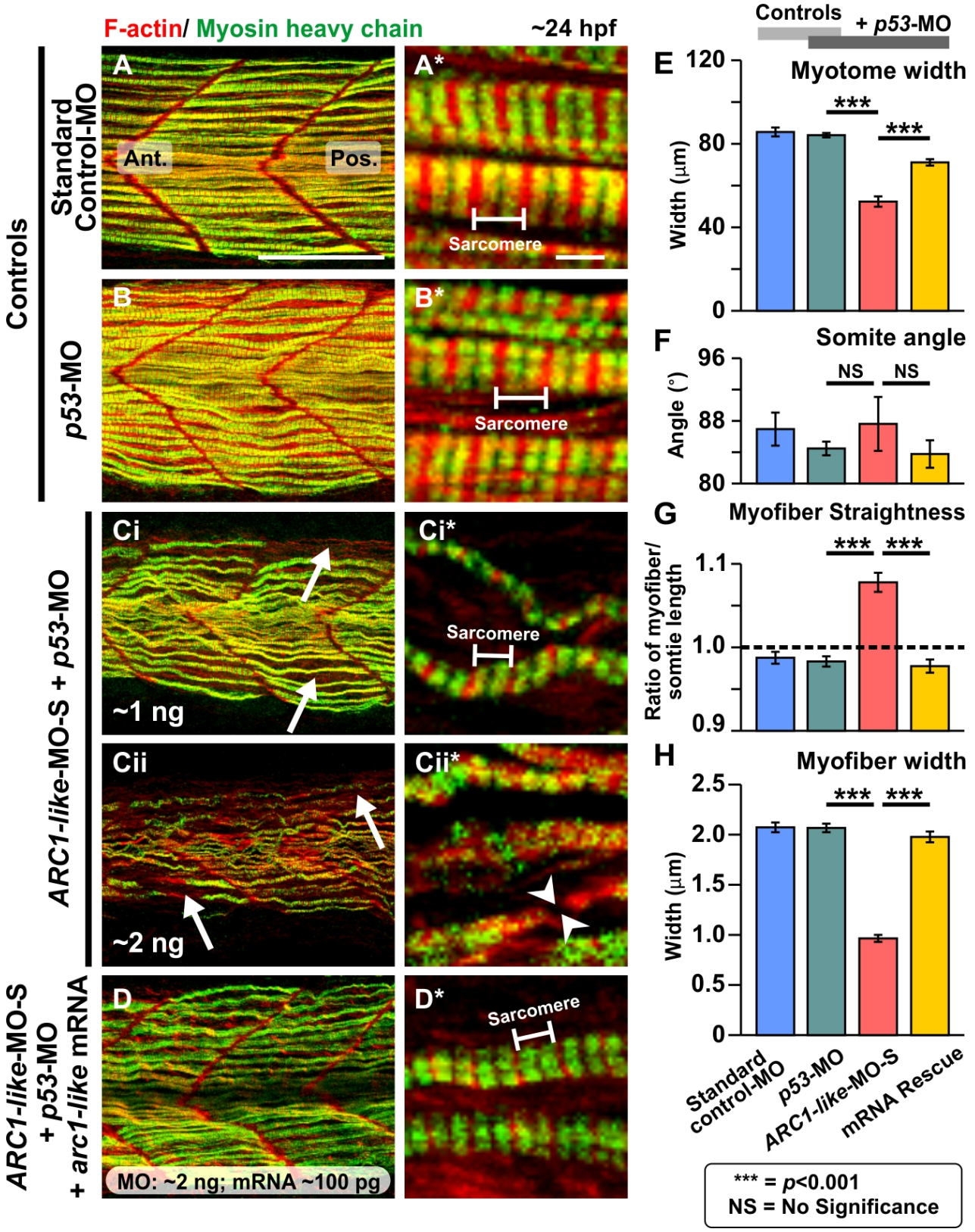
F-actin/ Myosin heavy chain
~24 hpf
Controls
Standard Control-MO
p53-MO
ARC1-like-MO-S + p53-MO
ARC1-like-MO-S + p53-MO + arc1-like mRNA
A
A*
Ant.
Pos.
Sarcomere
B
B*
Ci
Ci*
~1 ng
Cii
Cii*
~2 ng
D
D*
MO: ~2 ng; mRNA ~100 pg
Controls
+ p53-MO
E
Myotome width
Width (μm)
120
80
40
0
***
***
F
Somite angle
Angle (°)
96
88
80
NS
NS
G
Myofiber Straightness
Ratio of myofiber/ somtie length
1.1
1.0
0.9
***
***
H
Myofiber width
Width (μm)
2.5
2.0
1.5
1.0
0.5
0
***
***
Standard control-MO
p53-MO
ARC1-like-MO-S
mRNA Rescue
*** = p<0.001
NS = No Significance

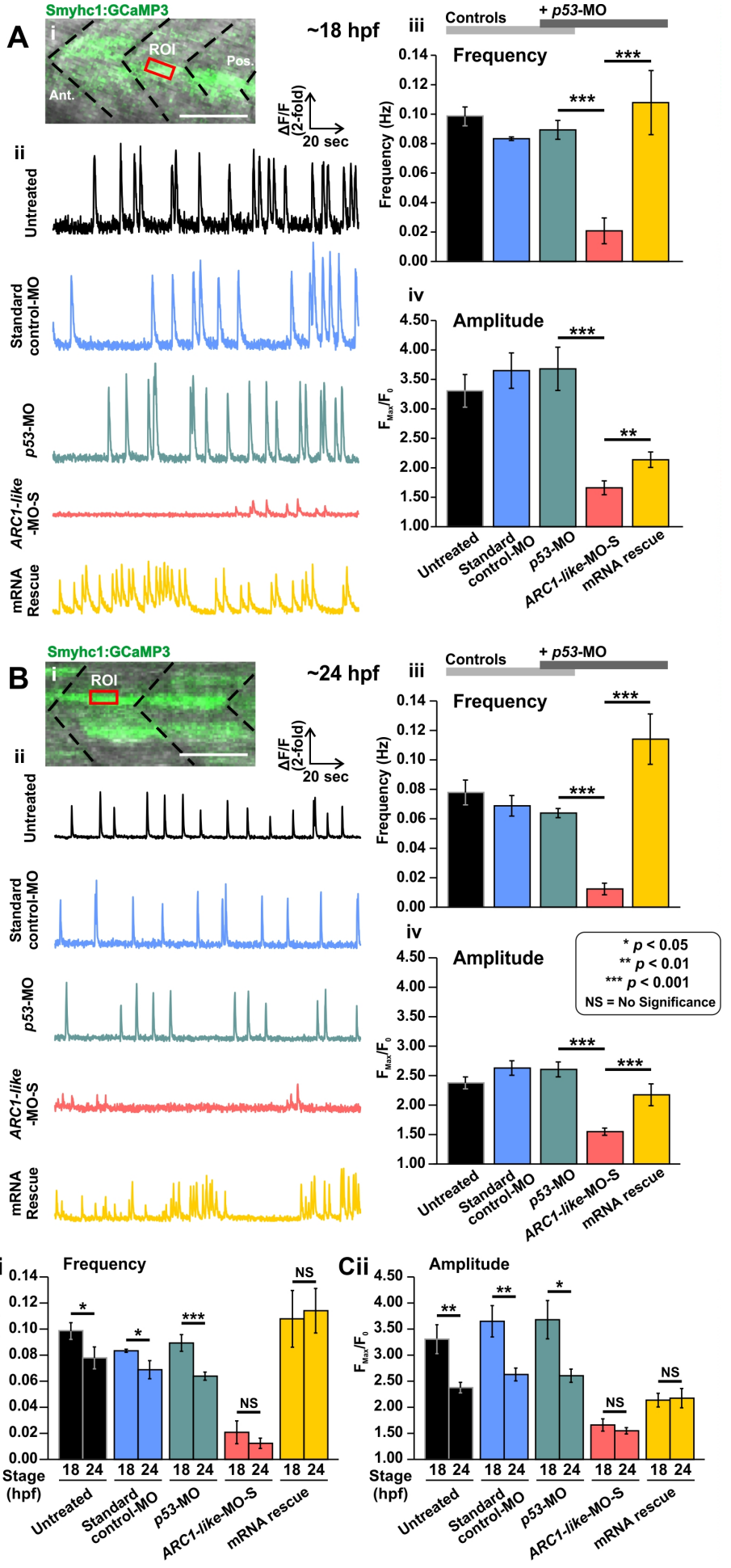
A
Smyhc1:GCaMP3
i
ROI
Pos.
Ant.
~18 hpf
ΔF/F (2-fold)
20 sec
ii
Untreated
Standard control-MO
p53-MO
ARC1-like -MO-S
mRNA Rescue
iii
Controls
+ p53-MO
Frequency
Frequency (Hz)
***
iv
Amplitude
F_Max/F_0
**
Untreated
Standard control-MO
p53-MO
ARC1-like-MO-S
mRNA rescue
B
Smyhc1:GCaMP3
~24 hpf
* p < 0.05
** p < 0.01
*** p < 0.001
NS = No Significance
Ci
Frequency
Cii
Amplitude
Stage (hpf)
18 24
NS

SUPPLEMENTARY INFORMATION

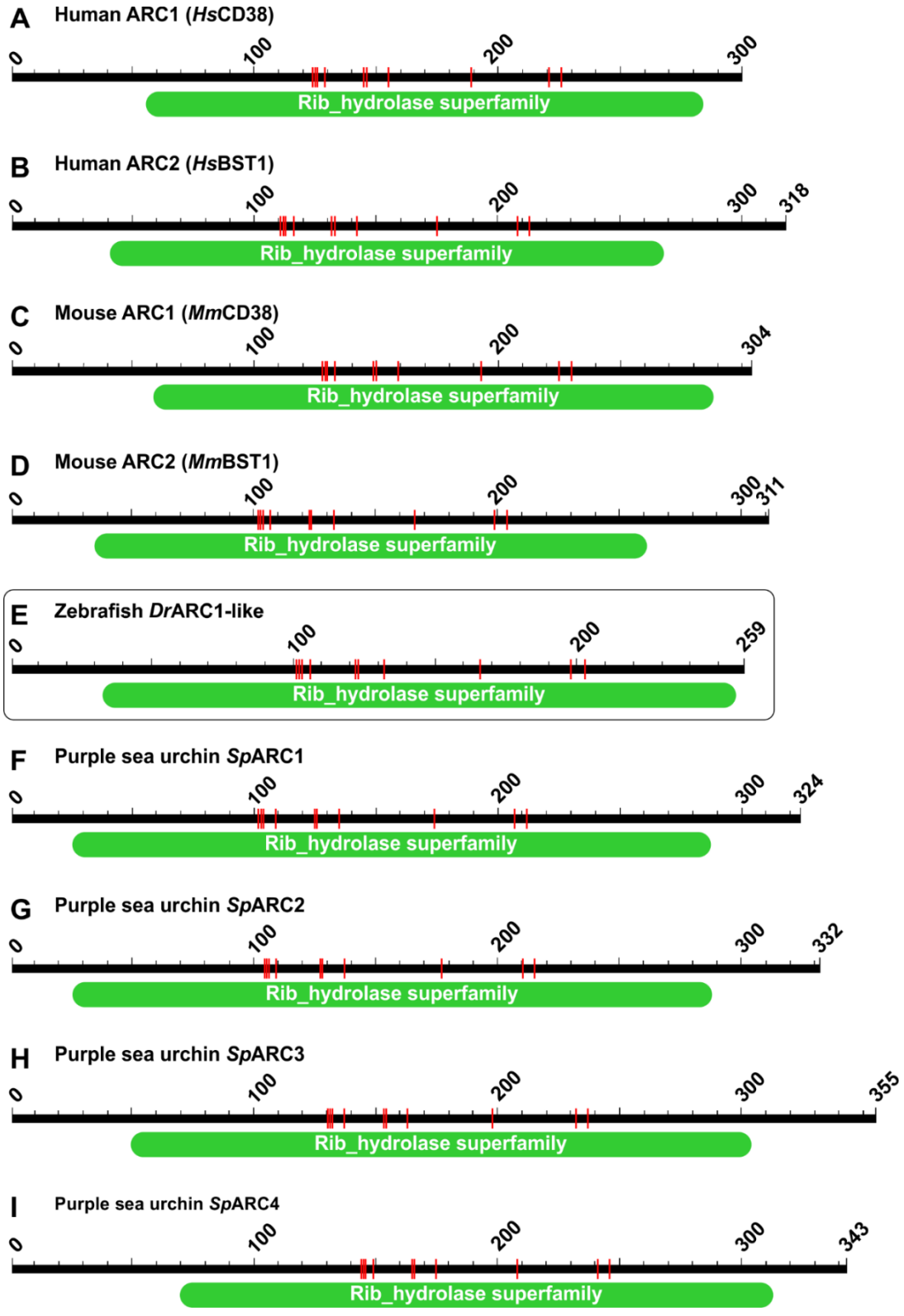

Fig. S1. Conserved domain architectures across the ARC homologs in various species. A conserved domain (i.e, Rib_hydrolase) was identified across the various ARC homologs using the NCBI Conserved Domain Search. The red lines indicate the ten residues that are important for substrate binding in this conserved Rib_hydrolase domain.

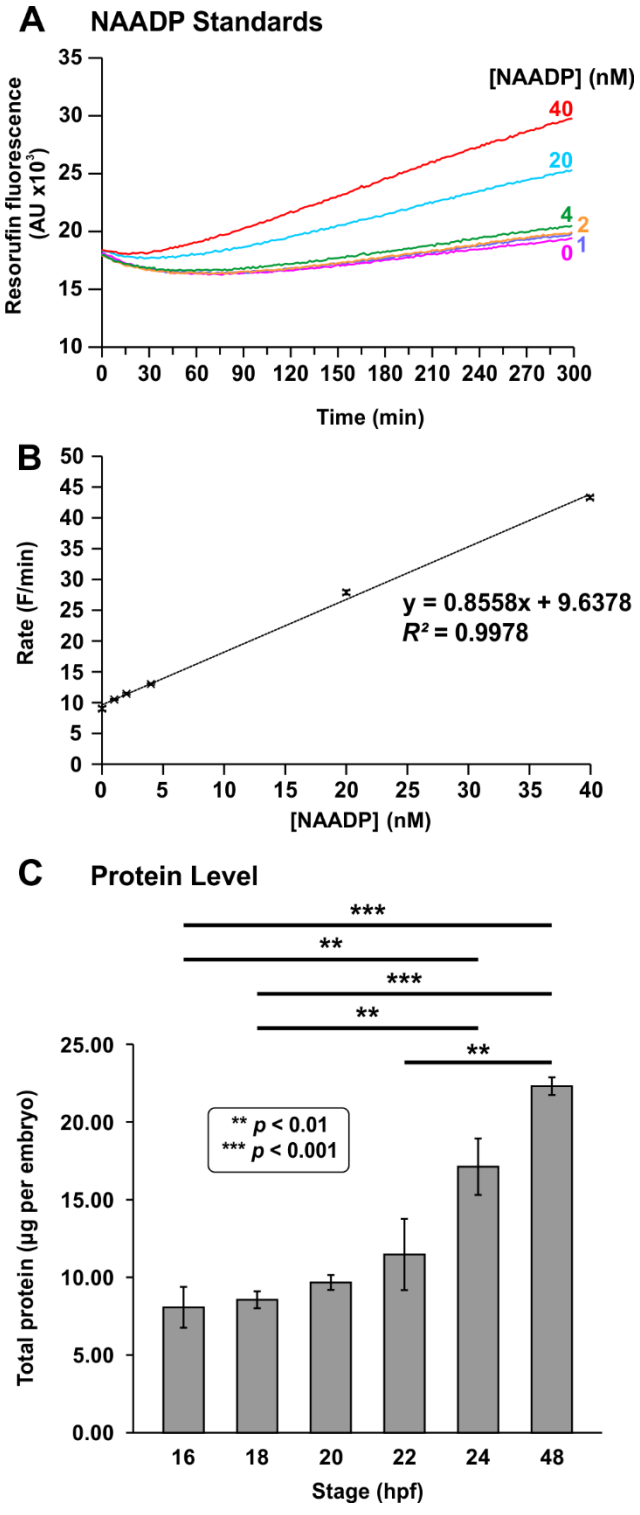

Fig. S2. Representative NAADP standard curve obtained from the NAADP cycling assay, and the total amount of protein in embryos measured at different stages of development. (A) Plot of resorufin

fluorescence over time in the NAADP standards at 0 nM, 1 nM, 2 nM, 4 nM, 20 nM, and 40 nM. **(B)** The reaction rate (i.e., the change in resorufin fluorescence over time), was plotted against [NAADP] (n=3 for each concentration) and then fitted into a linear regression model. **(C)** Bar graph showing the change in total level of protein (µg per embryo) at 16 hpf, 18 hpf, 20 hpf, 22 hpf, 24 hpf, and 48 hpf. The asterisks indicate statistically significant differences at $p<0.01$ (**) and $p<0.001$ (***).

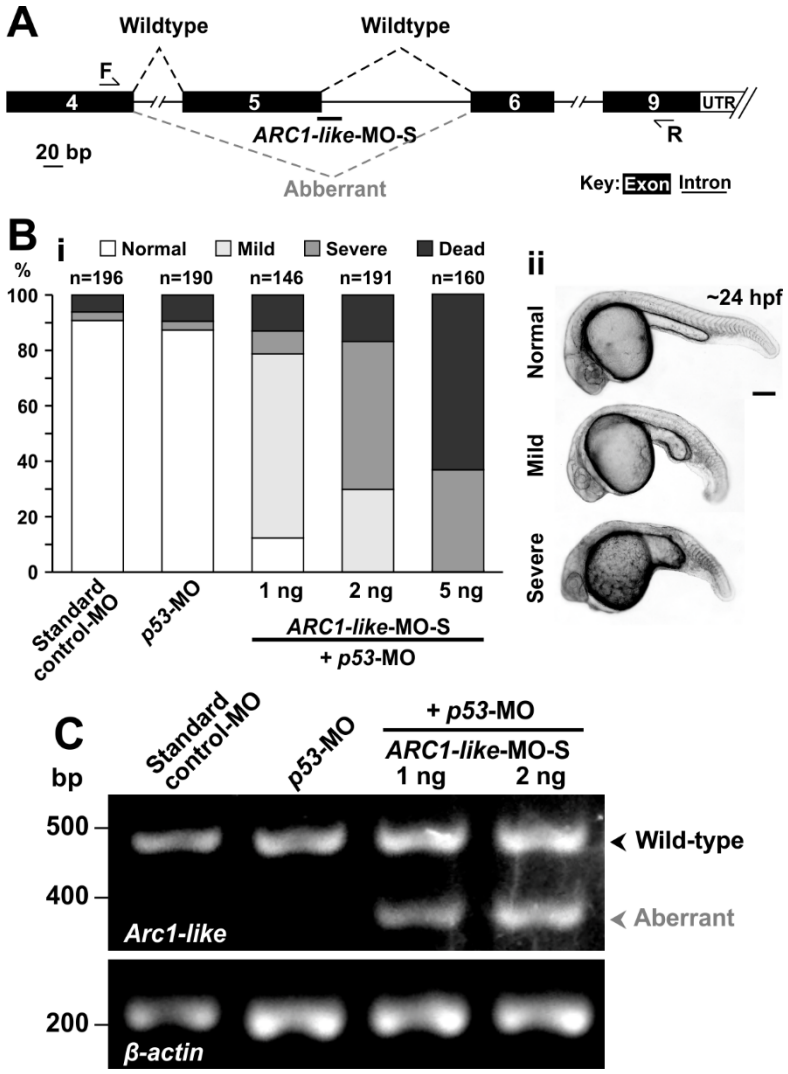

Fig. S3. MO-based knockdown of ARC1-like. (A) Design of the splice-interfering *ARC1-like*-MO-S. Scale bar, 20 bp. **(Bi)** Dose-response chart of the *ARC1-like*-MO-S. **(Bii)** Gross morphology of the ARC1-like morphants at ~24 hpf. Scale bar, 200 µm. **(C)** Evaluation of the knockdown efficacy of the *ARC1-like*-MO-S via RT-PCR and gel electrophoresis. *β-actin* was used as an internal control.

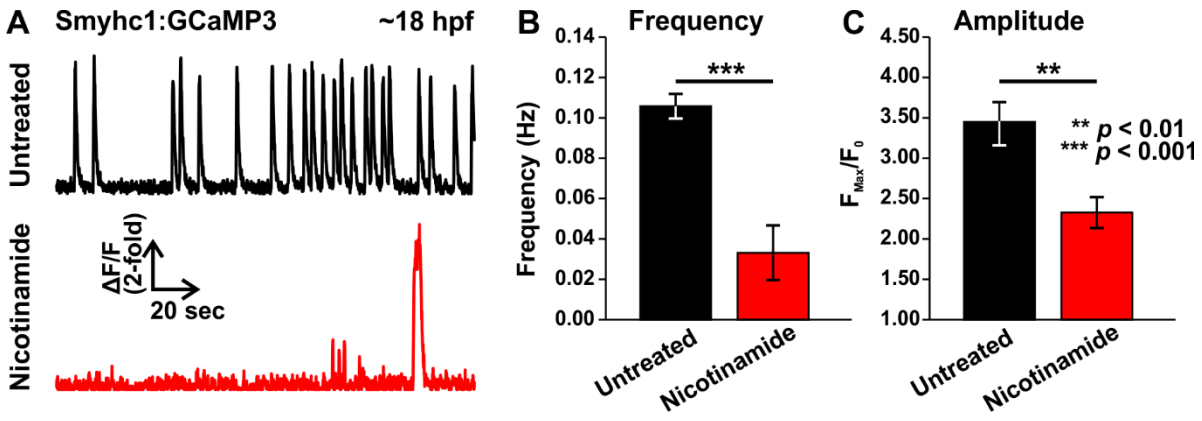

Fig. S4. Effect of nicotinamide on the Ca^{2+} signaling in slow muscle cells at ~18 hpf. Smyhc1:GCaMP3 transgenic embryos were tail-cut at ~17 hpf and then treated for 1 h with either Danieau's solution alone (untreated controls), or Danieau's solution containing 50 mM nicotinamide. **(A)** Representative line graphs showing the $\Delta F/F_0$ against time (over a period of ~180 sec) in the ROIs on selected slow muscle cells in the control and nicotinamide treatment groups at ~18 hpf. **(B,C)** Bar graphs to show the mean ± SEM **(B)** frequency and **(C)** amplitude of the Ca^{2+} transients at ~18 hpf (n=15-25, from 3-5 embryos). In panels **(B** and **C)**, the asterisks indicate statistically significant differences at $p<0.01$ (**) and $p<0.001$ (***).

SUPPLEMENTAL EXPERIMENTAL PROCEDURES

Phenotypic study of zebrafish embryos using bright-field and video microscopy

To study the gross morphology of zebrafish embryos, high resolution bright-field images were obtained as previously described (Kelu et al., 2017) using a Leica DFC290 camera mounted on a Zeiss Axioskop microscope using a Zeiss Plan-NEOFLUAR 5X/ 0.15 NA objective lens.

Measurement of protein concentration via the bicinchoninic acid (BCA) protein assay

The standard BCA protein assay was performed on sonicated embryo samples (collected at 16 hpf, 18 hpf, 20 hpf, 22 hpf, 24 hpf, and 48 hpf) after NAADP extraction to measure the mass of protein in each sample. In brief, protein pellets were resuspended in 100 mM NaOH and then sonicated on ice. The sonicated protein was then diluted by 1:10 or 1:100. In addition, a series of bovine serum albumin (BSA) standards at varying concentrations (i.e., 0, 10, 50, 100, 400, 800, and 1000 µg/mL) were prepared in 100 mM NaOH. Measurements were made by adding the diluted protein samples or the BSA standards to a working solution containing a 50:1 ratio of BCA and $CuSO_4$ at 4% w/v, and then incubated for 30 min at 37°C. To determine the concentration of protein, the absorbance of each reaction mixture was measured at 544 nm.

REFERENCE

Kelu, J.J., Webb, S.E., Parrington, J., Galione, A., and Miller, A.L. (2017). Ca^{2+} release via two-pore channel type 2 (TPC2) is required for slow muscle cell myofibrillogenesis and myotomal patterning in intact zebrafish embryos. *Dev. Biol.* **425**:109-129.